

# Topology-enhanced machine learning for consonant recognition

Yifei Zhu

[zhuuyf@sustech.edu.cn](mailto:zhuuyf@sustech.edu.cn)

Southern University of Science and Technology <https://orcid.org/0000-0001-8918-1896>

Pingyao Feng

Southern University of Science and Technology

Siheng Yi

Southern University of Science and Technology

Qingrui Qu

Southern University of Science and Technology

Zhiwang Yu

Southern University of Science and Technology

---

## Article

### Keywords:

**Posted Date:** March 12th, 2024

**DOI:** <https://doi.org/10.21203/rs.3.rs-3978261/v1>

**License:**  This work is licensed under a Creative Commons Attribution 4.0 International License.

[Read Full License](#)

**Additional Declarations:** There is **NO** Competing Interest.

---

# Topology-enhanced machine learning for consonant recognition

Pingyao Feng ✉, Siheng Yi, Qingrui Qu, Zhiwang Yu, Yifei Zhu ✉

1 **Abstract**—In artificial-intelligence-aided signal processing, existing  
 2 deep learning models often exhibit a black-box structure. The integration  
 3 of topological methods serves a dual purpose of making models  
 4 more interpretable as well as extracting structural information from time-  
 5 dependent data for smarter learning. Here, we provide a transparent  
 6 and broadly applicable methodology, TopCap, to capture topological  
 7 features inherent in time series for machine learning. Rooted in high-  
 8 dimensional ambient spaces, TopCap is capable of capturing features  
 9 rarely detected in datasets with low intrinsic dimensionality. Compared  
 10 to prior approaches, we obtain descriptors which probe finer information  
 11 such as the vibration of a time series. This information is then vectorised  
 12 and fed to multiple machine learning algorithms. Notably, in classifying  
 13 voiced and voiceless consonants, TopCap achieves an accuracy ex-  
 14 ceeding 96%, significantly outperforming traditional convolutional neural  
 15 networks in both accuracy and efficiency, and is geared towards design-  
 16 ing topologically enhanced convolutional layers for deep learning speech  
 17 and audio signals.

## 1 INTRODUCTION

18 IN 1966, Mark Kac asked the famous question: “Can you  
 19 hear the shape of a drum?” To hear the shape of a drum  
 20 is to infer information about the shape of the drumhead  
 21 from the sound it makes, using mathematical theory. In this  
 22 article, we venture to flip and mirror the question across  
 23 senses and address instead: “Can we see the sound of a  
 24 human speech?”

25 The artificial intelligence (AI) advancements have led to  
 26 a widespread adoption of voice recognition technologies,  
 27 encompassing applications such as speech-to-text conver-  
 28 sion and music generation. The rise of topological data  
 29 analysis (TDA) [1] has integrated topological methods into  
 30 many areas including AI [2, 3], which makes neural net-  
 31 works more interpretable and efficient, with a focus on  
 32 structural information. In the field of voice recognition  
 33 [4, 5], more specifically consonant recognition [6, 7, 8, 9,  
 34 10], prevalent methodologies frequently revolve around the  
 35 analysis of energy and spectral information. While topo-  
 36 logical approaches are still rare in this area, we combine  
 37 TDA and machine learning to obtain a classification for  
 38 speech data, based on geometric patterns hidden within  
 39 phonetic segments. The method we propose, TopCap (re-  
 40 ferring to capturing topological structures of data), is not  
 41 only applicable to audio data but also to general-purpose  
 42 time series data that require extraction of structural infor-  
 43 mation for machine learning algorithms. Initially, we endow

44 phonetic time series with point-cloud structure in a high-  
 45 dimensional Euclidean space via time-delay embedding  
 46 (TDE, see Fig. 1a) with appropriate choices of parameters.  
 47 Subsequently, 1-dimensional persistence diagrams are com-  
 48 puted using persistent homology (see Sec. S.2.2 for an expla-  
 49 nation of the terminologies). We then conduct evaluations  
 50 with nine machine learning algorithms, in comparison with  
 51 a convolutional neural network (CNN) without topological  
 52 inputs, to demonstrate the significant capabilities of TopCap  
 53 in the desired classification.

54 Conceptually, TDA is an approach that examines data  
 55 structure through the lens of topology. This discipline was  
 56 originally formulated to investigate the *shape* of data, par-  
 57 ticularly point-cloud data in high-dimensional spaces [11].  
 58 Characterised by a unique insensitivity to metrics, robust-  
 59 ness against noise, invariance under continuous deforma-  
 60 tion, and coordinate-free computation [1], TDA has been  
 61 combined with machine learning algorithms to uncover in-  
 62 tricate and concealed information within datasets [12, 3, 13,  
 63 14, 15, 16]. In these contexts, topological methods have been  
 64 employed to extract structural information from the dataset,  
 65 thereby enhancing the efficiency of the original algorithms.  
 66 Notably, TDA excels in identifying patterns such as clusters,  
 67 loops, and voids in data, establishing it as a burgeoning tool  
 68 in the realm of data analysis [17]. Despite being a nascent  
 69 field of study, with its distinctive emphasis on the shape  
 70 of data, TDA has led to novel applications in various far-  
 71 reaching fields, as evidenced in the literature. These include  
 72 image recognition [18, 19, 20], time series forecasting [21]  
 73 and classification [22], brain activity monitoring [23, 24],  
 74 protein structural analysis [25, 26], speech recognition [27],  
 75 signal processing [28, 29], neural networks [30, 31, 32, 2],  
 76 among others. It is anticipated that further development of  
 77 TDA will pave a new direction to enhance numerous aspects  
 78 of daily life.

79 The task of extracting features that pertain to structural  
 80 information is both intriguing and formidable. This process  
 81 is integral to a multitude of practical applications [33, 34,  
 82 35, 36], as scholars strive to identify the most effective  
 83 representatives and descriptors of shape within a given  
 84 dataset. Despite the fact that TDA is specifically designed  
 85 for shape capture, there are several hurdles that persist in  
 86 this newly developed field of study. These include (1) the  
 87 nature and sensitivity of descriptors obtained by methods in  
 88 TDA, (2) the dimensionality of the data and other parameter

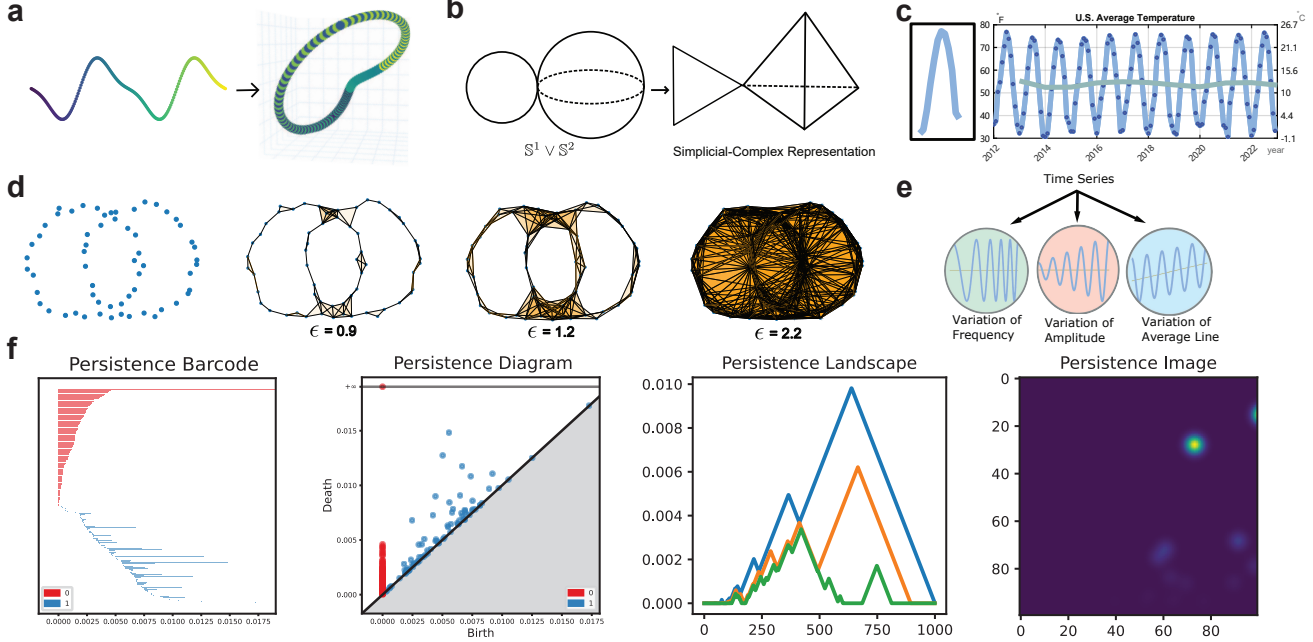


Fig. 1: Illustrations of methodology. **a**, Time-delay embedding (dimension=3, delay=10, skip=1) of  $f(t_n) = \sin(2t_n) - 3\sin(t_n)$ , with  $t_n = \frac{\pi}{50}n$  ( $0 \leq n \leq 200$ ). Resulting point clouds lay on a closed curve in 3-dimensional Euclidean space. The colour indicates their original locations in the time series. **b**, A topological space and its triangulation. On the left is a topological space consisting of a 1-dimensional sphere (i.e., a circle) and a 2-dimensional sphere with a single point of contact, denoted as  $S^1 \vee S^2$ . The right depicts a triangulation of this topological space. **c**, Average temperature in the U.S. with monthly values (dark blue dots) and yearly values (green curve). The left panel shows a single-year section of average temperature. **d**, Computing PH. The four plots consecutively show how a diagram or a barcode is computed: Connect each pair of points with a distance less than  $\epsilon$  by a line segment, fill in each triple of points with mutual distances less than  $\epsilon$  with a triangular region, etc., and compute the corresponding homology groups. In this way, as “time”  $\epsilon$  increases, points in the diagram or intervals in the barcode record the “birth” and “death” of each generator of a homology group, i.e., the occurrence and disappearance of a loop (or a higher-dimensional hole), thereby revealing the essential topological features of the point cloud that persist. **e**, Characterising the vibration of a time series in terms of its variability of frequency, amplitude, and average line. **f**, Commonly used representations for PH, with an example of 100 points uniformly distributed over a bounded region in 2D Euclidean space.

choices, (3) the vectorisation of topological features, and (4) computational cost. These challenges will be elaborated in the following paragraphs within this section. Subsequently, we will demonstrate how our proposed methodology, Top-Cap, addresses these challenges through an application to consonant classification.

When applying TDA, the most imminent question is to comprehend the characteristics and nature of descriptors extracted via topological methods. TDA is grounded in the pure-mathematical field of algebraic topology (AT) [37, 38], with persistent homology (PH) being its primary tool [39, 40]. While AT can quantify topological information to a certain extent [38, 1, 17], it is vitally important to understand both the capabilities and limitations of TDA. Generally speaking, TDA methods distinguish objects based on continuous deformation. For example, PH cannot differentiate a disk from a filled rectangle, given that one can continuously deform the rectangle into a disk by pulling out its four edges. In contrast, PH can distinguish between a filled rectangle and an unfilled one due to the presence of a “hole” in the latter, preventing a continuous deformation between the two. In certain circumstances, these methods are considered

excessively ambiguous to capture the structural information in data, thereby necessitating a more precise descriptor of shapes. To draw an analogy, TDA can be conceptualised as a scanner with diverse inputs encompassing time series, graphs, pictures, videos, etc. The output of this scanner is a multiset of intervals in the extended real line, referred to as a persistence diagram (PD)<sup>1</sup> or a persistence barcode (PB) [11, 41, 42] (cf. Fig. 1f). In particular, by *maximal persistence* (MP) we mean the maximal length of the intervals. The precision of the topological descriptor depends on two factors: (1) the association of a topological space, i.e., the process of transforming the input data into a topological space (see Fig. 1b for a simplicial-complex representation of spaces; typically, the original datasets are less structured, and one should find a suitable representation of the data), and (2) the vectorisation of PD or PB, i.e., how to perform statistical inference with PD/PB. Despite there are many theoretical results which provide a solid foundation for TDA, few can elucidate the practical implications of PD and PB. For exam-

<sup>1</sup>In this article, we shall freely use the usual birth-by-death PDs and their birth-by-lifetime variants, whichever better serve our purposes. See Sec. S.2.2 for details.

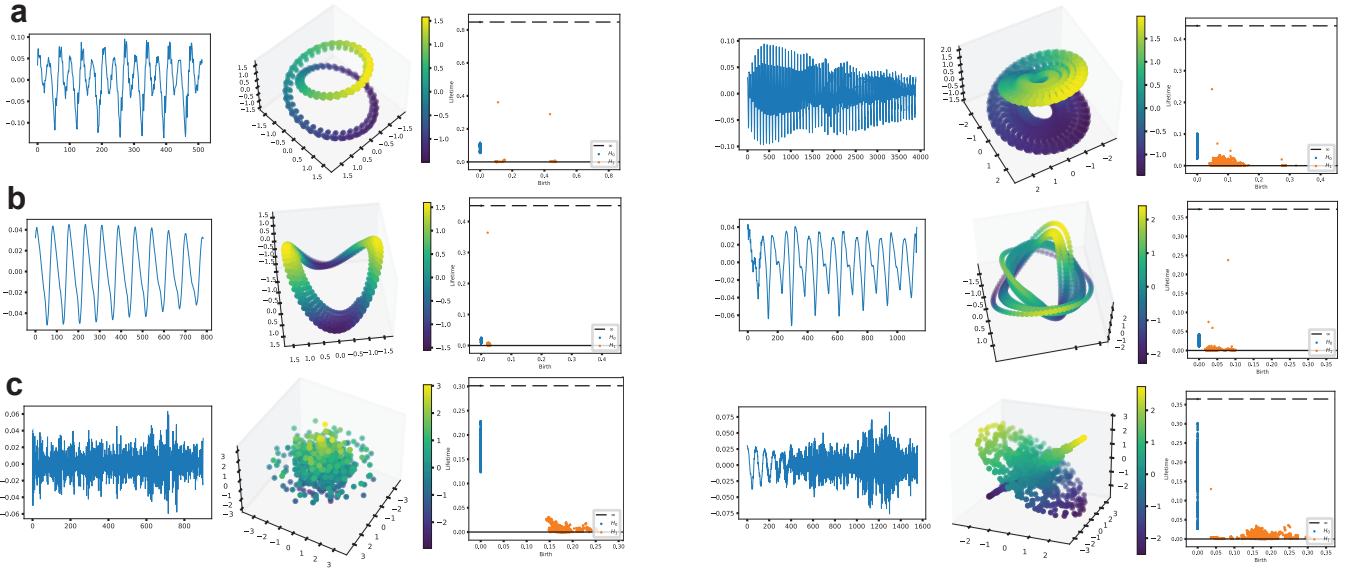


Fig. 2: The varied shapes of vowels, voiced consonants, and voiceless consonants. **a**, the left 3 panels and the right 3 panels depict 2 vowels, respectively. For each, the first picture is the time series of the vowel, the second picture corresponds to the 3-dimensional principal component analysis of the point cloud resulting from performing TDE (dimension=100, delay=1, skip=1) on this time series, and the third picture is the PD of this point cloud. **b**, The analogous features for 2 voiced consonants. **c**, Those for 2 voiceless consonants.

ple, what does it mean if many points are distributed near the birth-death diagonal line in a PD? In most cases, these points are regarded as descriptors of noise and are often disregarded if possible. Consequently, the TDA scanner can be seen as an imprecise observer, overlooking much of the information contained in less significant regions. In this article, we present an example of simulated time series to demonstrate that points distributed in such regions indeed encode vibration patterns of the time series, and a different distribution in these regions leads to a different pattern of vibration. This serves as a motivation for proposing TopCap and is further discussed in Sec. 2.1. It turns out that topological descriptors can be sharpened by noting patterns in these regions.

In view of the capability of topological methods to discern vibration patterns in time series, we apply them to classify consonant signals into voiced and voiceless categories. As a first demonstration of our findings, to visualise vowels, voiced consonants, and voiceless consonants in TDE and PD, see Fig. 2 (cf. Sec. S.1 for details of phonetic categories).

The first challenge, as many researchers may encounter when applying topological methods, is to determine the dimension of point clouds derived from input data [43, 44, 45]. This essentially involves transforming the input into a topological space. In situations where the dimensionality of the data is large, researchers often project the data into a lower-dimensional topological space to facilitate visualisation and reduce computational cost [23, 24, 46]. On the other hand, as in this study and other applications with time series analysis [47, 48, 49, 50, 22, 51, 27], low-dimensional data are embedded into a higher-dimensional space. In both scenarios, deciding on the data dimensionality is both critical and challenging. Often, tuning the dimension is a tremendous task. In Sec. 3 of Discussion below, we delve

into the issue of data dimensionality. In our case, as it might seem counterintuitive compared to most algorithms, when the data are embedded into a higher-dimensional space, the computation will be a little faster, the point cloud appears smoother and more regular, and most importantly, more salient topological features can be spotted, which seldom happen in lower-dimensional spaces. When encountering the dimensionality of data, researchers would think of the well-known curse of dimensionality [52]: As a typical algorithm grapple, with the increase of dimension, more data are needed to be involved, often growing exponentially and thereby escalating computational cost. Even worse, the computational cost of the algorithm itself normally rises as the dimension goes higher. However, topological methods do not necessarily prefer data of lower dimension. For computing PH (see Fig. 1d for the process of computing PD/PB from point clouds), a commonly used algorithm [53, 54] sees complexity grow with an increase in the number  $n$  of simplices during the process, with a worst-case polynomial time-complexity of  $O(n^3)$ . As such, the computational cost is directly related to the number of simplices formed during filtration. Our observation shows that computation time may not increase much given an increase of dimension of data, because the latter may have little effect on the size (i.e., number of points) of the point cloud and thus neither on the number of simplices formed during filtration.

Having obtained a suitable topological space from input data, one can derive a PD/PB from the topological space, which constitutes a multiset of intervals. The subsequent challenge lies in the vectorisation of the PD/PB for its integration into a machine-learning algorithm. The vectorisation process is essentially linked to the construction of the topological space, as the combination of different methods for constructing the topological space and vectori-

199 sation together determine the descriptor utilised in machine  
 200 learning. A plethora of vectorisation methods exist, such  
 201 as persistence landscape (PL) [55] and persistence image  
 202 (PI) [56], among others, as documented in various studies  
 203 [40, 57] (cf. Fig. 1f). The selection of these methods requires  
 204 careful consideration. In Sec. 4 of Methods, we employ MP  
 205 and its corresponding birth time as two features. These  
 206 have been integrated into nine traditional machine learning  
 207 algorithms to classify voiced and voiceless consonants,  
 208 yielding an accuracy that exceeds 96% with each algorithm.  
 209 This vectorisation method is quite simple, primarily due to  
 210 our construction of topological spaces from phonetic time  
 211 series, as detailed in the Method section. This construction  
 212 enables PH to capture significant topological features within  
 213 the time series. In Sec. 2.1, we also observe a pattern of  
 214 vibration which could potentially be vectorised by PI into a  
 215 matrix. As one of its strengths, PI emphasises regions where  
 216 the weighting function scores are high, which makes it a  
 217 computationally flexible method. Future work may involve  
 218 a more precise recognition of such patterns using PI.

219 An outline for the remainder of this article goes as fol-  
 220 lows. Sec. 1.1 gives an overview of closely related works in  
 221 the field, with an extended commentary relegated to Sec. S.4.  
 222 Sec. 2 of Results provides in more detail the motivations  
 223 for TopCap, presents final results of classifying voiced and  
 224 voiceless consonants, including a comparison with tradi-  
 225 tional deep learning neural networks, and explains our  
 226 purposes in practical use. Sec. 3 of Discussion highlights im-  
 227 portant parameter setups and indicates potential directions  
 228 for future work, with further discussion in Sec. S.3. Sec. 4  
 229 of Methods contains a detailed template of TopCap. Sec. 5  
 230 gives the data and code sources for our experiments.

### 231 1.1 Related works

232 Time series analysis [58] is a prevalent tool for various  
 233 applied sciences. The recent surge in TDA has opened new  
 234 avenues for the integration of topological methods into time  
 235 series analysis [21, 59, 60]. Much literature has contributed  
 236 to the theoretical foundation in this area. For example,  
 237 theoretical frameworks for processing periodic time series  
 238 have been proposed by Perea and Harer [61], followed by  
 239 their and their collaborators' implementation in discovering  
 240 periodicity in gene expressions [62]. Their article [61] stud-  
 241 ied the geometric structure of truncated Fourier series of a  
 242 periodic function and its dependence on parameters in time-  
 243 delay embedding (TDE), providing a solid background for  
 244 TopCap. In addition to periodic time series, towards more  
 245 general and complex scenarios, quasi-periodic time series  
 246 have also been the subject of scholarly attention. Research  
 247 in this direction has primarily concentrated on the selection  
 248 of parameters for geometric space reconstruction [63] and  
 249 extended to vector-valued time series [64].

250 In this article, a topological space is constructed from  
 251 data using TDE, a technique that has been widely em-  
 252 ployed in the reconstruction of time series (see Fig. 1a and  
 253 cf. Sec. S.2.1 for more background). Thanks to the topolog-  
 254 ical invariance of TDE, the general construction of simplicial  
 255 complex representation (see Fig. 1b) and computation of PH  
 256 from point clouds (see Fig. 1d) apply to time series data,

257 although this transformation involves subtle technical issues  
 258 in practice. For instance, Emrani et al. utilised TDE and PH  
 259 to identify the periodic structure of dynamical systems, with  
 260 applications to wheeze detection in pulmonology [47]. They  
 261 selected the embedded dimension  $d$  as 2, and their delay para-  
 262 meter  $\tau$  was determined by an autocorrelation-like (ACL)  
 263 function, which provided a range for the delay between the  
 264 first and second critical points of the ACL function. Pereira  
 265 and de Mello proposed a data clustering approach based  
 266 on PD [48]. The data were initially reconstructed by TDE,  
 267 with  $d = 2$  and  $\tau = 3$ , so as to obtain the corresponding  
 268 PD, which was then subjected to  $k$ -means clustering. The  
 269 delay  $\tau$  was determined using the first minimum of an  
 270 auto mutual information, and the embedded dimension  $d$   
 271 was set to be 2 as using 3 dimensions did not significantly  
 272 improve the results. Khasawneh and Munch introduced a  
 273 topological approach for examining the stability of a class  
 274 of nonlinear stochastic delay equations [49]. They used false  
 275 nearest neighbours to determine the embedded dimension  
 276  $d = 3$  and chose the delay to equal the first zeros of the  
 277 ACL function. Subsequently, the longest persistence lifetime  
 278 in PD was used as a vectorisation to quantify periodicity.  
 279 Umeda focused on a classification problem for volatile time  
 280 series by extracting the structure of attractors, using TDA  
 281 to represent transition rules of the time series [22]. He  
 282 assigned  $d = 3$ ,  $\tau = 1$  in his study and introduced a novel  
 283 vectorisation method, which was then applied to a con-  
 284 volutional neural network (CNN) to achieve classification.  
 285 Gidea and Katz employed TDA to detect early signs prior  
 286 to financial crashes [51]. They studied multi-dimensional  
 287 time series with  $\tau = 1$  and used persistence landscape as  
 288 a vectorisation method. For speech recognition, Brown and  
 289 Knudson examined the structure of point clouds obtained  
 290 via TDE of human speech signals [27]. The TDE parameters  
 291 were set as  $d = 3$ ,  $\tau = 20$ , after which they examined the  
 292 structure of point clouds and their corresponding PB.

293 Upon reviewing the relevant literature, we see that  
 294 currently there is no general framework for systematically  
 295 choosing  $d$  and  $\tau$ , and researchers often have to make  
 296 choices in an ad hoc fashion for practical needs. While the  
 297 TDE-PH topological approach to handling time series data  
 298 is not new, TopCap extracts features from high-dimensional  
 299 spaces. For example, in our experiment  $d = 100$ . It happens  
 300 in some cases that in a low-dimensional space, regardless  
 301 of how optimal the choice of  $\tau$  is, the structure of the time  
 302 series cannot be adequately captured. In contrast, given a  
 303 high-dimensional space, feature extraction from data be-  
 304 comes simpler. Of course, operating in a high-dimensional  
 305 space comes with its own cost. For example, the adjustment  
 306 of  $\tau$  then requires careful consideration. Nonetheless, it also  
 307 offers advantages, which we will elucidate step by step in  
 308 the subsequent sections.

## 2 RESULTS

309 This research drew inspiration from Carlsson and his col-  
 310 laborators' discovery of the Klein-bottle distribution of high-  
 311 contrast, local patches of natural images [20], as well as their  
 312 subsequent recent work on topological CNNs for learning  
 313 image and even video data [2]. By analogy, we aim to  
 314 understand a distribution space for speech data, even a

316 directed graph structure on it modeling the complex net-  
 317 work of speech-signal sequences for practical purposes such  
 318 as speaker diarisation, and how these topological inputs  
 319 may enable smarter learning (cf. Sec. S.1). Here are some  
 320 of our first findings in this direction, set in the context of  
 321 topological time series analysis.

## 322 2.1 Detection of vibration patterns

323 The impetus behind TopCap lies in an observation of how  
 324 PD can capture vibration patterns within time series. To  
 325 begin with, our aim is to determine which sorts of in-  
 326 formation can be extracted using topological methods. As  
 327 the name indicates, topological methods quantify features  
 328 based on topology, which distinguishes spaces that cannot  
 329 continuously deform to each other. In the context of time  
 330 series, we conduct a series of experiments to scrutinise the  
 331 performance of topological methods, their limitations as  
 332 well as their potential.

333 Given a periodic time series, its TDE target is situated on  
 334 a closed curve (i.e., a loop) in a sufficiently high-dimensional  
 335 Euclidean space (see Fig. 1a). Despite the satisfactory point-  
 336 cloud representation of a periodic time series, it remains  
 337 rare in practical measurement and observation to capture  
 338 a truly periodic series. Often, we find ourselves dealing with  
 339 time series that are not periodic yet exhibit certain pat-  
 340 terns within some time segments. For instance, Fig. 1c  
 341 portrays the average temperature of the United States from  
 342 the year 2012 to 2022, as documented in [65]. Although the  
 343 temperature does not adhere strictly to a periodic pattern,  
 344 it does display a noticeable cyclical trend on an annual  
 345 basis. Typically, the temperature tends to rise from January  
 346 to July and fall from August to December, with each year  
 347 approximately comprising one cycle of the variation pat-  
 348 tern. One strength of topological methods is their ability  
 349 to capture “cycles”. A question then arises naturally: Can  
 350 these methods also capture the cycle of temperature as well  
 351 as subtle variations within and among these cycles? To  
 352 be more precise, we first observe that variations occur in  
 353 several ways. For instance, the amplitude (or range) of the  
 354 annual temperature variation may fluctuate slightly, with  
 355 the maximum and minimum annual temperatures varying  
 356 from year to year. Additionally, the trend line for the annual  
 357 average temperature also shows fluctuations, such as the  
 358 average temperature in 2012 surpassing that of 2013. Despite  
 359 each year’s temperature pattern bearing resemblance to  
 360 that depicted in the left panel in Fig. 1c (representing a  
 361 single cycle of temperature within a year), it may be more  
 362 beneficial for prediction and response strategies to focus on  
 363 the evolution of this pattern rather than its specific form. In  
 364 other words, attention should be directed towards how this  
 365 cycle varies over the years. This leads to several questions.  
 366 How can we consistently capture these subtle changes in  
 367 the pattern’s evolution, such as variations in the frequency,  
 368 amplitude, and trend line of cycles? How can we describe  
 369 the similarities and differences between time series that  
 370 possess distinct evolutionary trajectories? In applications,  
 371 these are crucial inquiries that warrant further exploration.

372 To address these questions, we propose three kinds of  
 373 “fundamental variations” which are utilised for depicting  
 374 the evolutionary trace of a time series. Consider a series of  
 375 a periodic function  $f(t_n) = f(t_n + T)$ , where  $T$  is a period.

- (1) *Variation of frequency.* Denote the frequency by  $F = T^{-1}$ .  
 Note that the series is not necessarily periodic in the  
 mathematical sense. Rather, it exhibits a recurring pat-  
 tern after the period  $T$ . For instance, the average tem-  
 perature from Fig. 1c is not a periodic series, but we  
 consider its period to be one year since it follows a  
 specific pattern, i.e., the one displayed in the left panel of  
 Fig. 1c. This 1-year pattern always lasts for a year as time  
 progresses. Hence, there is no frequency variation in this  
 example. This type of variations can be represented as  

$$g_1(t_n) = f(F(t_n) \cdot t_n),$$
 where  $F(t_n)$  is a series repre-  
 senting the changing frequency. This type of variation  
 occurs, for example, when one switches their vocal tone  
 or when one’s heartbeats experience a transition from  
 walking mode to running mode.
- (2) *Variation of amplitude.* The amplitudes of temperature  
 in the years 2014 and 2015 are  $42.73^{\circ}\text{F}$  and  $40.93^{\circ}\text{F}$ ,  
 respectively. So the variation of amplitude from 2014 to  
 2015 is  $-1.80^{\circ}\text{F}$ . This can be represented by  $g_2(t_n) =$   

$$A(t_n) \cdot f(t_n),$$
 where  $A(t_n)$  is a series of the changing  
 amplitude. This type of variation is observed when  
 a particle vibrates with resistance or when there is a  
 change in the volume of a sound.
- (3) *Variation of average line.* The average temperatures  
 through the years 2012 and 2013 are  $55.28^{\circ}\text{F}$  and  $52.43^{\circ}\text{F}$ ,  
 respectively. The variation of average line from 2012 to  
 2013 is  $-2.85^{\circ}\text{F}$ . Let  $g_3(t_n) = f(t_n) + L(t_n)$ , where  $L(t_n)$   
 is a series representing the variation of average line. This  
 type of variation is observed when a stock experiences  
 a downturn over several days or when global warming  
 causes a year-by-year increase in temperature.

To summarise, Fig. 1e provides a visual representation of  
 the three fundamental variations. It is important to note  
 that these variations are not utilised to depict the pattern  
 itself but rather to illustrate the variation within the pattern  
 or how the time series oscillates over time. This approach  
 offers a dynamic perspective on the evolution of the time  
 series, capturing changes in patterns that static analyses  
 may overlook.

Using three simulated time series corresponding to the  
 above three fundamental types of variation (see Sec. 4.1 for  
 detailed construction), we demonstrate that PD can distin-  
 guish these variations and detect how significant they are.  
 See Fig. 3, where a smaller value of  $c$  indicates a more rapid  
 fundamental variation. Here, regardless of which value  $c$   
 takes, each individual diagram features a prominent single  
 point at the top and a cluster of points with relatively short  
 duration, except when  $F(t_n) = 1$  (i.e.,  $c = 4$ ). In this case,  
 the series represents a cosine function, and thus the diagram  
 consists of a single point. Normally, one tends to overlook  
 the points in a PD that exhibit a short duration as they  
 are sometimes inferred as noise. However, in this example,  
 the distribution of those points holds valuable information  
 regarding the three fundamental variations. As shown in  
 Fig. 3, each fundamental variation has its distinct pattern  
 of distribution in the lower region of a diagram, which  
 leads to refined inferences: If the points spiral along the  
 vertical axis of lifetime, it is probably due to a variation  
 of amplitude; if every two or four points stay close to form  
 a “shuttle”, it probably indicates a variation of average line;

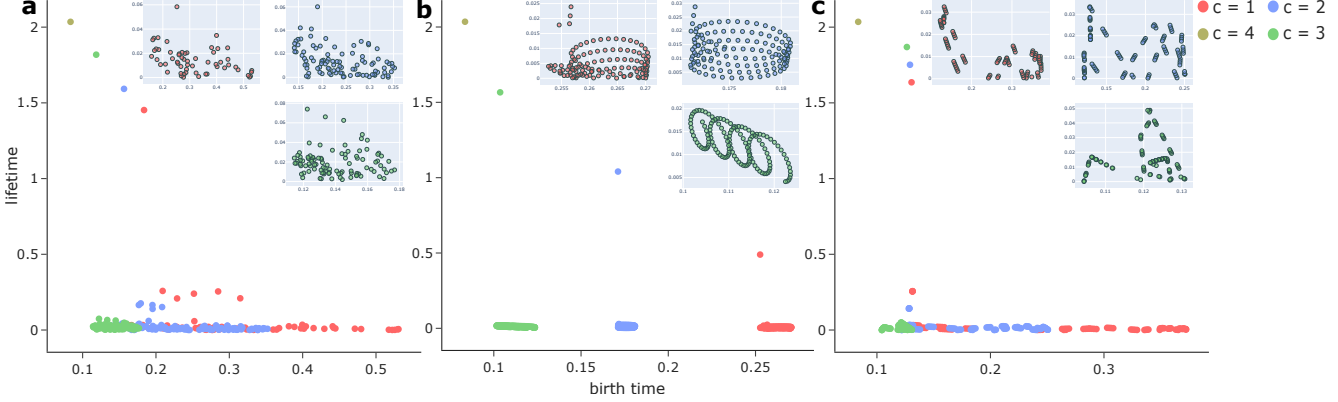


Fig. 3: 1-dimensional PH reveals three fundamental variations. **a**, Detecting variation of frequency. Upper-right panels zoom in to show the barcode distribution in the lower dense region, where the position and colour of each value of  $c$  in the main legend corresponds to those of its panel. Note that when  $c = 4$ , there is a single point, and so the panel for this value is omitted. **b**, Detecting variation of amplitude. **c**, Detecting variation of average line.

otherwise the points just seem to randomly spread over, which more likely results from a variation of frequency. It is also straightforward to distinguish the values of  $c$  for a specific fundamental variation, by their most significant point in the diagram: Longer lifetime for the barcode of the solitary point indicates slower variation. The lower region of a diagram also gives some hints in this respect.

In this simulated example, we demonstrated how PD could be utilised as a uniform means to distinguish three fundamental variations of the cosine series and their respective rates of change. However, it is important to note that in general scenarios, identifying the fundamental variations in a time series using topological methods may encounter significant challenges. Although topological methods are indeed capable of capturing this information, vectorising this information for subsequent utilisation remains a complex task at this stage. Having recognised the potential of topological methods, we resort to an alternative algorithm for handling time series. Specifically, despite the difficulty in vectorising PD to measure each fundamental variation, we have developed a simplified algorithm to measure the vibration of time series as a whole. This approach provides a comprehensive understanding of the overall behaviour of a time series, bypassing the need for complex vectorisation.

## 460 2.2 Traditional machine learning methods with novel 461 topological features

462 Using datasets comprising human speech, we initially employ the Montreal Forced Aligner to align natural speech  
463 into phonetic segments. Following preprocessing of these  
464 phonetic segments, TDE is conducted with dimension pa-  
465 rameter  $d = 100$  and delay parameter  $\tau$  set to equal  $6T/d$ ,  
466 where  $T$  approximates the (minimal) period of the time  
467 series. Following additional refinement procedures, PDs are  
468 computed for these segments and are then vectorised based  
469 on MP and its corresponding birth time. The comprehensive  
470 procedural framework is expounded in Secs. 4.2 and 4.3,  
471 while the corresponding workflow is shown in Fig. 4e.  
472 In the applications of TDE, the dimension parameter  $d$  is  
473 usually determined through some algorithms designed to

475 identify the minimal appropriate dimension [45, 66]. The  
476 delay parameter  $\tau$  is determined by an ACL function with  
477 no specific rule, but in many cases  $\tau = mT/d$  for some  
478 positive integer  $m$ . In our pursuit of enhanced extraction of  
479 topological features, a relatively high dimension is chosen  
480 (see Sec. 3 for more discussion on dimension in TDE).  
481 Given this higher dimension, the usual case of  $\tau = T/d$   
482 with  $m = 1$  may prove excessively diminutive, particularly  
483 in light of the time series only taking values in discrete  
484 time steps. Consequently, in TopCap we adopt an adjusted  
485 parametrisation for  $\tau = mT/d$  with a relatively large value  
486  $m = 6$ .

487 We input the pair of MP and birth time from 1-  
488 dimensional PD for each sound record to multiple tradi-  
489 tional classification algorithms: Tree, Discriminant, Logis-  
490 tic Regression, Naive Bayes, Support Vector Machine,  
491 k-Nearest Neighbours, Kernel, Ensemble, and Neural Net-  
492 work. We use the application of the MATLAB (R2022b) Clas-  
493 sification Learner, with 5-fold cross-validation, and set aside  
494 30% records as test data. This application performs machine  
495 learning algorithms in an automatic way. There are a total  
496 of 1016 records, with 712 training samples and 304 test  
497 samples. Among them, 694 records are voiced consonants  
498 and the remaining are voiceless consonants. The models we  
499 choose in this application are Optimizable Tree, Optimizable  
500 Discriminant, Efficient Logistic Regression, Optimizable  
501 Naive Bayes, Optimizable SVM, Optimizable KNN, Kernel,  
502 Optimizable Ensemble, and Optimizable Neural Network.  
503 Our results are compared with those obtained from a CNN,  
504 for which we compute the short-time Fourier transform  
505 of phones (implemented in Python with `signal.stft` or  
506 `scipy.signal.spectrogram`) and directly classify the  
507 resulting spectrograms using CNN, without extracting any  
508 topological features.

509 The results are shown in Fig. 4a-d. The receiver op-  
510 erating characteristic curve (ROC), area under the curve  
511 (AUC), and accuracy metrics collectively demonstrate the  
512 efficacy of these topological features as inputs for a variety  
513 of machine learning algorithms. Each of the algorithms  
514 incorporating topological inputs attains AUC and accuracy  
515 surpassing 96%, whereas CNN without topological inputs

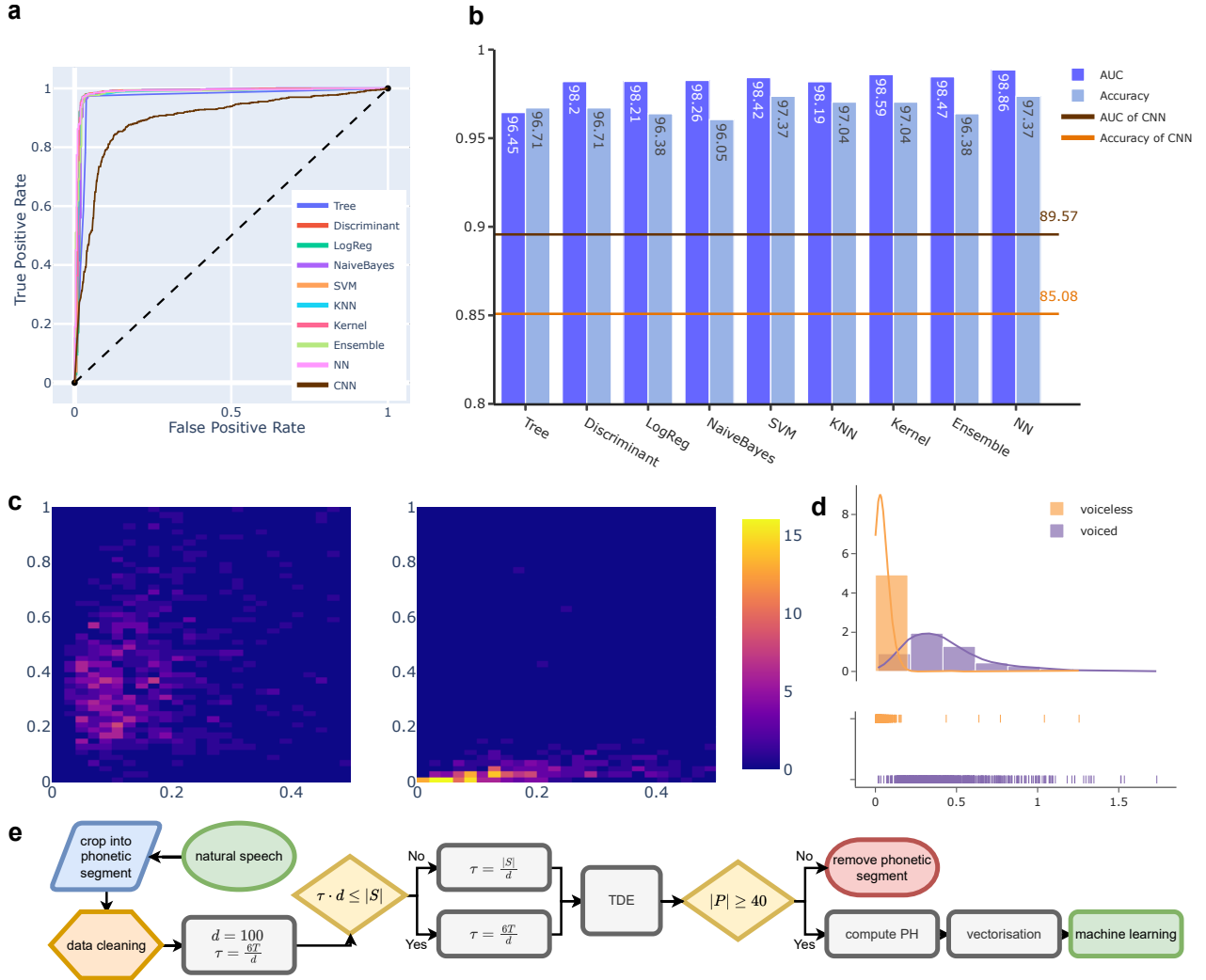


Fig. 4: Machine learning results with topological features. **a**, ROCs of TopCap’s traditional machine learning algorithms with topological inputs and of CNN without topological inputs. **b**, Accuracy and AUC of TopCap versus CNN. **c**, Diagrams of records represented as (birth time, lifetime) for voiced consonants (left) and voiceless consonants (right), where voiced consonants exhibit relatively higher birth time and lifetime. The colour represents the density of points in each unit grid box. **d**, Histograms of records represented by their lifetime for voiced and voiceless consonants, together with kernel density estimation and rug plot. The distributions of MP can distinguish voiced and voiceless consonants. **e**, Flow chart of experiment. Here  $|S|$  denotes the number of samples in a time series,  $|P|$  denotes the number of points in the point cloud, and  $T$  denotes the (minimal) period of the time series computed by the ACL function.

merely yields an AUC of 90% and an accuracy of 85%. The ROC and AUC together depict the high performance of our classification model across all classification thresholds. The 2D histograms depicted in Fig. 4c-d collectively illustrate the distinct distributions of voiced and voiceless consonants. Voiced consonants tend to exhibit a relatively higher birth time and lifetime, which provides an explanation for the high performance of these algorithms. Despite the intricate structure that a PD may present, appropriately extracted topological features enable traditional machine learning algorithms to separate complex data effectively. This highlights the potential of TDA in enhancing the performance of machine learning models.

It is noteworthy that the CNN we use as a comparative, which comprises 5 layers with more than 43 million

parameters, is considerably more intricate than traditional machine learning algorithms with TopCap. Nonetheless, in effect, this CNN requires 2 hours for sufficient training (1602 spectrograms in total). In contrast, learning with topological inputs achieves both higher accuracy as in Fig. 4a-b and higher efficiency, under 5 minutes including topological feature extraction on the same device (mere seconds for machine learning alone).

In summary, from our topological detection results, the most significant distinction between voiced and voiceless consonants is that the former exhibit higher MP. This can scarcely be detected in lower dimensions regardless of how we tune the delay parameter  $\tau$ . Besides the figure above, see also Fig. 2 for a sample of the recognition of vowels as well as consonants in terms of their shapes.

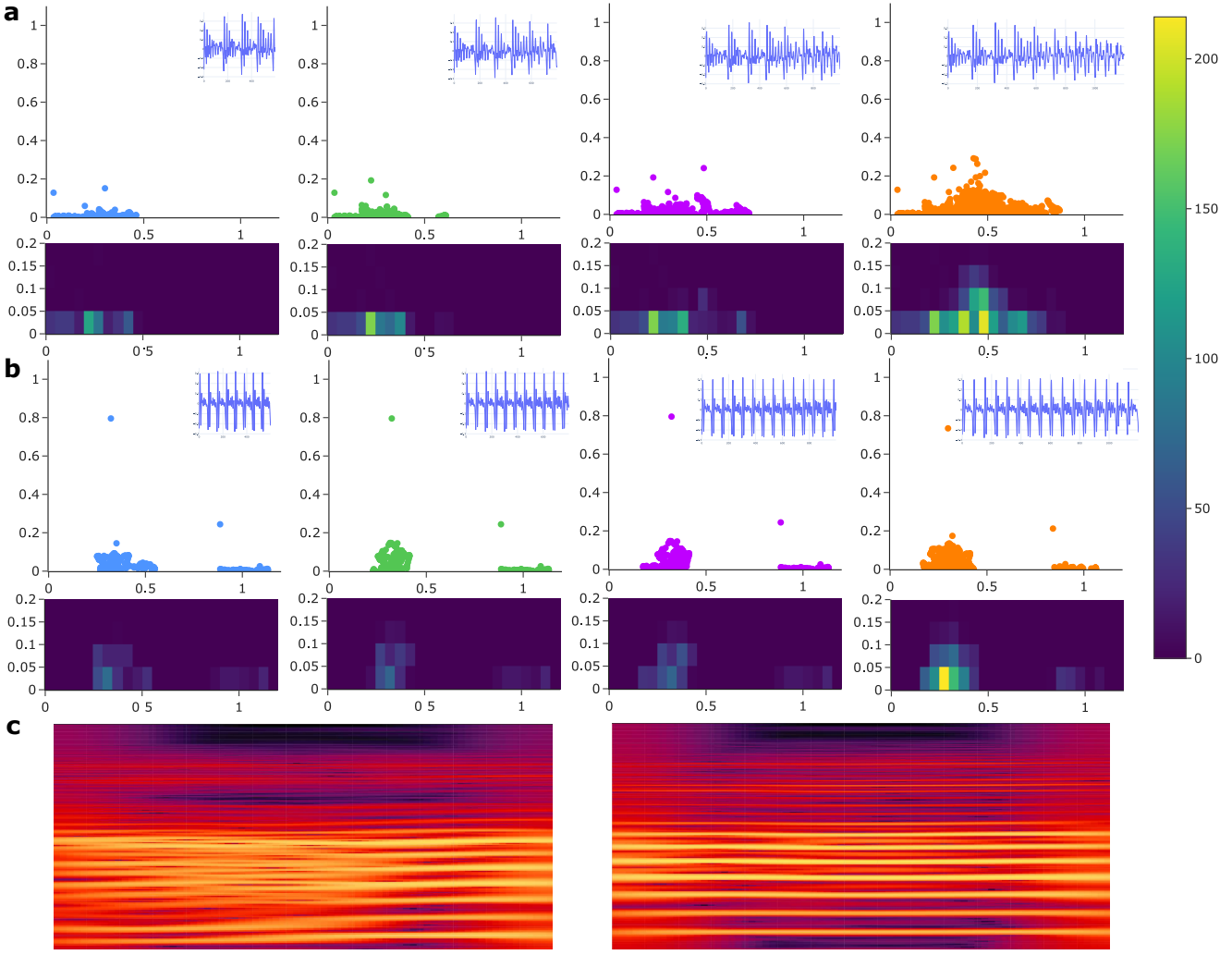


Fig. 5: Variation of 1-dimensional PDs due to the fundamental variations of time series. **a**, PDs of drastic fundamental variations. The small panel on top right of each diagram shows the original time series, with 4 segments extracted from the same record of [ɑ], each starting from time 0 and ending at time 600, 800, 1000, 1200, respectively. It can directly be seen from the time series that the variation of amplitude in (a) is bigger than (b); for frequency, see c; normally, we do not discuss the average line of phonetic data as it is assumed to be constant. Below, each diagram shows the clustering density of points in the lower region of the PD. **b**, PDs of mild fundamental variations for 4 time-series segments extracted from the other record of [ɑ], with the same ending and starting times as in (a). The lower density diagrams demonstrate that unstable time series are characterised by a higher density of points in the lower region of PD. Moreover, stable series tend to attain high MP. **c**, Spectral frequency plots of the time series with rapid variations (left) and with mild variations (right).

### 546 2.3 The three fundamental variations gleaned from a 547 persistence diagram

548 A PD for 1-dimensional PH encodes much more information  
549 beyond the birth time and lifetime of the point of MP.  
550 The three fundamental variations examined in Sec. 2.1 also  
551 manifest themselves in certain regions of the PD, which can  
552 in turn be vectorised.

553 To capture these variations, we perform an experiment  
554 with two records of the vowel [ɑ]. Specifically, we demon-  
555 strate the fundamental variations by comparing the PDs  
556 of (a) the record of [ɑ] relatively unstable with respect to  
557 the fundamental variations and (b) the other record of the  
558 same vowel that is relatively stable. To better illustrate the

559 results, we crop each record into 4 overlapping intervals,  
560 each starting from time 0 and ending at 600, 800, 1000, 1200,  
561 respectively. When adding a new segment of 200 units into  
562 the original sample each time, the amplitude and frequency  
563 of the series altered more drastically in case (a). A more  
564 rapid changing rate may lead to more points distributed  
565 in the lower region of the diagram. The outcomes are  
566 presented in Fig. 5. The plots in Fig. 5c show that the spectral  
567 frequency of (a) indeed varies faster than that of (b).

568 We should also mention that the 1-dimensional PD here  
569 serves as a profile for the collective effect of the fundamental  
570 variations. Currently, it is unclear how the points in the  
571 lower region change in response to a specific variation.

### 572 3 DISCUSSION

573 In the realm of applying topological methods to analyse  
 574 time series [47, 48, 49, 50, 22, 51, 27], the determination of  
 575 parameters for TDE emerges as a pivotal aspect. This stems  
 576 from the significant impact that the selection of parameters  
 577 has on the resulting topological spaces and their corre-  
 578 sponding PDs. There exist several convenient algorithms for  
 579 parameter selection. For example, the False Nearest Neigh-  
 580 bours algorithm (FNN), a widely utilised tool, provides a  
 581 method for deciding the minimal embedded dimension [66].  
 582 However, in the context of PH, usually the objective is not  
 583 to achieve a *minimal* dimension. Contrarily, a dimension  
 584 of substantial magnitude may be desirable due to certain  
 585 advantages it offers.

586 In this section, as a main novel feature of TopCap, we  
 587 reveal and leverage the relationship between embedded  
 588 dimension and maximal persistence. We relegate further  
 589 aspects of parameter selection to Sec. S.3.

590 In the TDE-PH approach, the determination of dimen-  
 591 sion in a TDE can be complex. However, it plays a pivotal  
 592 role in the extraction of topological descriptors such as  
 593 MP. It is observed that a larger dimension can significantly  
 594 enhance the theoretically optimal MP of a time series. In  
 595 TopCap, the dimension of TDE is set to be 100, a relatively  
 596 large dimension for the experiment. On the other hand,  
 597 several factors also constrain this choice. These include  
 598 the length of the sampled time series, since the dimension  
 599 cannot exceed the length (otherwise it would render the  
 600 resulting point cloud literally pointless). The constraints also  
 601 include the periodicity of the time series, as the time-delay  
 602 window size should be compatible with the approximate  
 603 period of the time series, which is to be elaborated below.

604 According to Perea and Harer [61, Proposition 5.1], there  
 605 is no information loss for trigonometric polynomials if and  
 606 only if the dimension of TDE exceeds twice the maximal fre-  
 607 quency. Here, no information loss implies that the original  
 608 time series can be fully reconstructed from the embedded  
 609 point cloud. In general, for a periodic function, a higher  
 610 dimension of TDE can yield a more precise approxima-  
 611 tion by trigonometric polynomials. Although there are no  
 612 absolutely periodic functions in real data, each time series  
 613 exhibits its own pattern of vibration, as discussed in Sec. 2.1,  
 614 and a higher dimension of embedding may be employed  
 615 to capture a more accurate vibration pattern in the time  
 616 series. Furthermore, an increased embedded dimension may  
 617 result in reduced computation time for PD. For instance,  
 618 computation times for a voiced consonant [η] are 0.2671,  
 619 0.2473, and 0.2375 seconds, corresponding to embedded  
 620 dimensions 10, 100, and 1000 (see Fig. 6a). This is attributed  
 621 to the reduction due to a higher dimension on the number  
 622 of points in the embedded point cloud. While this reduction  
 623 in computation time may not be considered substantial  
 624 compared to the impact of changing skip (see Fig. 6d), it  
 625 may become significant when handling large datasets. More  
 626 importantly, an increased embedded dimension can yield  
 627 benefits such as enhanced MP, which serves as a major moti-  
 628 vation for higher dimensions, as well as a smoother shape  
 629 of resulting point clouds obtained through TDE, which  
 630 makes the embedding visibly reasonable. Typically, for most  
 631 algorithms, a lower dimension is preferred due to factors

632 such as those associated with curse of dimensionality and  
 633 computation cost. By contrast, in TopCap, we opt instead  
 634 for a higher dimension.

635 However, the embedded dimension cannot be arbitrarily  
 636 large. As illustrated in Fig. 6c, when the embedded dimen-  
 637 sion escalates to 1280, it becomes unfeasible to capture a  
 638 significant MP in the phonetic time series. This results from  
 639 a break of the point cloud. When the embedded dimension  
 640 further reaches 1290, an empty 1-dimensional barcode is  
 641 obtained due to the lack of points necessary to form even  
 642 a single cycle. In this way, the dimension of TDE is related  
 643 to the length of the time series.

644 Using a sound record of the voiced consonant [η] as  
 645 an exemplar, we delineate the correlation between MP and  
 646 embedded dimension in Fig. 6a–c. As depicted in Fig. 6b,  
 647 MP tends to escalate rapidly and nonlinearly with the  
 648 increase in dimension, signifying that a more substantial  
 649 MP is captured in higher-dimensional TDE. Notably, two  
 650 precipitous drops in MP are observed, corresponding to  
 651 embedded dimensions 600 and 1190. When  $d = 600$ , this  
 652 time series can theoretically attain its optimal MP when  
 653  $\tau = 2$  (see Sec. S.2.1). However, given the length of the series  
 654 is 1337 and the window size is  $d \cdot \tau = 1200$ , with the skip  
 655 set as 5, only 28 points are in the resulting point cloud for  
 656 PD computation. The sparse point cloud fails to represent  
 657 the original series adequately, leading to a decrease in MP.  
 658 A similar phenomenon occurs when the dimension reaches  
 659 1190. The principal component analysis for dimension 1280  
 660 is shown in Fig. 6c. In this scenario, as observed above,  
 661 the hypothetical cycle fails to form as there is a break in  
 662 the point cloud, resulting in a free-fall in MP. In contrast,  
 663 when  $d = 630$ , this series has a significant MP when  $\tau = 1$ ,  
 664 resulting in a window size of  $d \cdot \tau = 630$ . There are 142 points  
 665 in the point cloud for the persistence diagram if skip equals  
 666 5, ensuring that the MP rises again without any breakdown.  
 667 The embedded dimension also contributes significantly to  
 668 the geometric property of time-delay embedding, as the  
 669 shape becomes smoother in higher dimensions and the  
 670 point cloud more structural.

671 As mentioned above, there are three crucial parameters  
 672 in TDE, namely,  $d$ ,  $\tau$ , and skip. However, it is worth noting  
 673 that the TDE-PH approach encompasses many other signif-  
 674 icant variables and choices. These include the construction  
 675 of underlying topological space of the point clouds (i.e., the  
 676 distance function for pairwise points), and the type of com-  
 677 plexes utilised in filtering PH, among others. Some of these  
 678 choices, despite their importance, were seldom addressed in  
 679 the literature. Here, we propose a method for determining  
 680 delay in order to capture the theoretically optimal MP of a  
 681 time series in high-dimensional TDE. In future research, we  
 682 aim at more systematic approaches for determining other  
 683 parameters, particularly dimension of the TDE.

### 684 4 METHODS

#### 685 4.1 Constructing vibrating time series

686 There are three kinds of fundamental variations mentioned  
 687 in Sec. 2.1. In order to substantiate our argument, let  $t_n =$

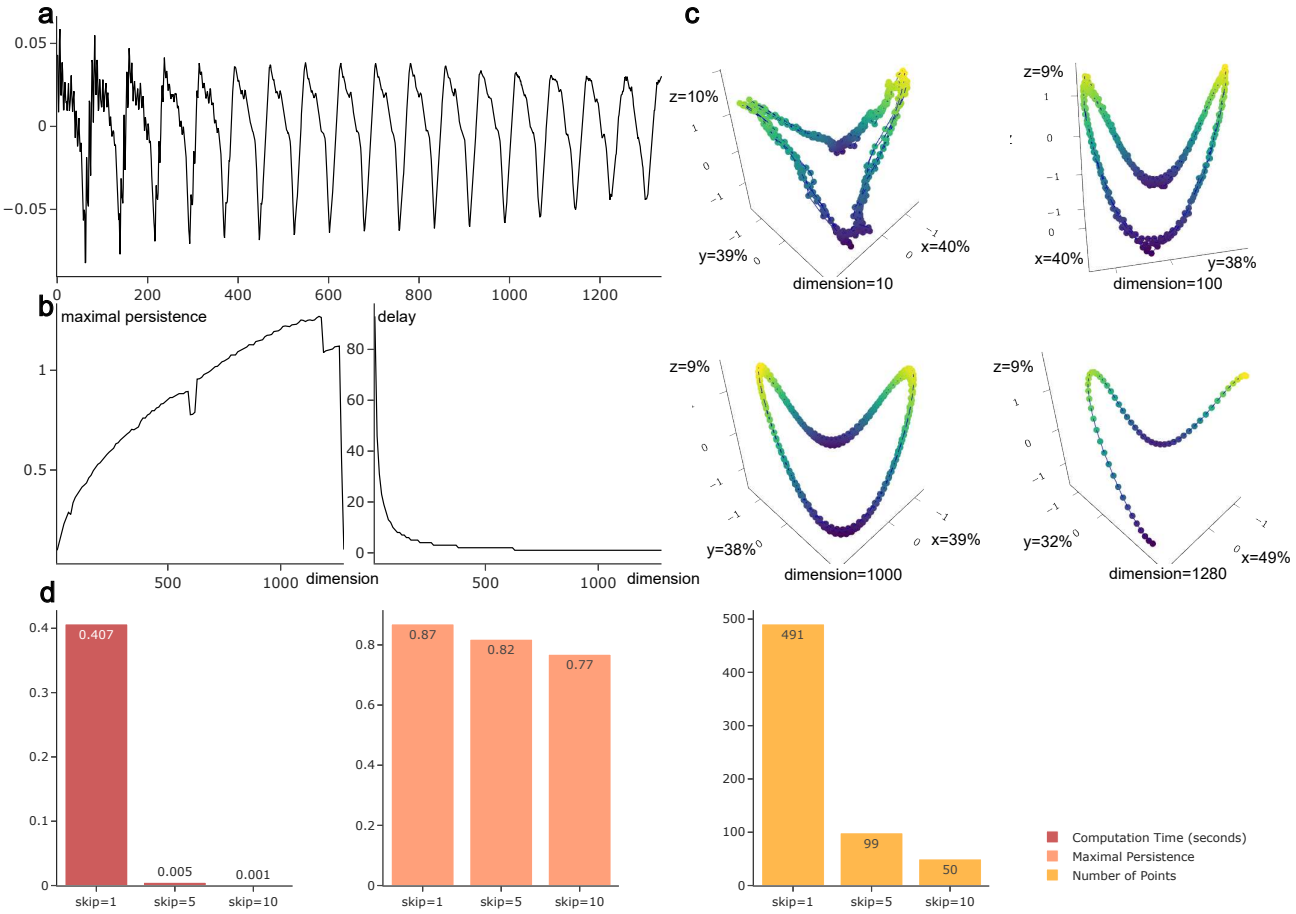


Fig. 6: Point-cloud behaviour with increasing embedded dimension. **a**, Original .wav file of a record of [m] (voiced consonant). **b**, MP of the series after TDE as dimension increases (left) and the corresponding delay that ensures the time series to reach theoretically optimal MP (right). Skip equals 5 when computing PD. **c**, Visualisation of the embedded point clouds, which shows principal component analysis (PCA) of the embedded point clouds in 3D as projected from various dimensions. Skip equals 1 when performing PCA. The percentage along each axis indicates the PCA explained variance ratio. **d**, Given a sound record of the voiced consonant [m], computation time, MP, and the size of point clouds as skip increases (see Sec. S.3.1 for details). An increase in skip can lead to a significant reduction in computation time, owing to the reduced size of the point cloud. However, MP remains resilient to an increase in the skip parameter.

688 0.01n with  $0 \leq t_n \leq 7\pi$  and for each  $c \in \{1, 2, 3, 4\}$  define

$$\begin{aligned} f(t_n) &= \cos(t_n) \\ F(t_n) &= \frac{c}{4} + \frac{1 - \frac{c}{4}}{7\pi} \cdot t_n \\ g_1(t_n) &= f(F(t_n) \cdot t_n) \end{aligned}$$

689 Note that  $F(t_n) = c/4$  when  $t_n = 0$  and  $F(t_n) = 1$  when  
690  $t_n = 7\pi$ . In fact,  $F(t_n)$  is a sequence of line segments connecting  
691  $(0, c/4)$  and  $(7\pi, 1)$ . Correspondingly, the frequency  
692 of  $g_1(t_n)$  changes more slowly as  $c$  increases. In the extreme  
693 case when  $c = 4$ , we have  $F(t_n) = 1$ , so

$$g_1(t_n) = f(F(t_n) \cdot t_n) = f(t_n) = \cos(t_n)$$

694 which is a periodic function. For each value of  $c$ , we applied  
695 TDE to the series  $g_1(t_n)$  with dimension 3, delay 100, skip  
696 10 and computed the 1-dimensional PD of the embedded  
697 point cloud. See Fig. 3a for the results. Replacing  $F(t_n)$  by  
698  $A(t_n)$  and  $L(t_n)$ , we obtained the diagrams in Figs. 3b and  
699 3c, respectively.

## 4.2 Obtaining phonetic data from natural speech

We used speech files sourced from SpeechBox [67], ALLSTAR Corpus, task HT1 language English L1 file, retrieved on 28th January 2023. SpeechBox is a web-based system providing access to an extensive collection of digital speech corpora developed by the Speech Communication Research Group in the Department of Linguistics at Northwestern University. This section contains a total of 25 individual files, comprising 14 files from women and 11 files from men. The age range of these speakers spans from 18 to 26 years, with an average of 19.92. Each file is presented in the WAV format and is accompanied by its corresponding aligned file in Textgrid format, which features three tiers of sentences, words, and phones. Collectively, these 25 speech files amount to a total duration of 41.21 minutes. The speech file contains each individual reading the same sentences consecutively for a duration ranging from 80 to 120 seconds, contingent upon each person's pace. The original .wav file has a sampling frequency of 22050 and comprises only one channel. Since the Montreal Forced Aligner (MFA) [68]

720 is trained in a sampling frequency of 16000, we opted to  
 721 adjust the sampling frequency of the .wav files accordingly.  
 722 We then extracted the “words” tier from Textgrid and  
 723 aligned words into phones using English\_MFA dictionary  
 724 and acoustic model (MFA version 2.0.6). Thus we obtained  
 725 corresponding phonetic data from these speech files.

726 Subsequently, we used voiced and voiceless consonants  
 727 in those segments as our dataset. Voiced consonants are  
 728 consonants for which vocal cords vibrate in the throat during  
 729 articulation, while voiceless consonants are pronounced  
 730 otherwise (see also Sec. S.1). Specifically, using Praat [69], we  
 731 extracted voiced consonants [ŋ], [m], [n], [j], [l], [v], and [ʒ];  
 732 for voiceless consonants, we selected [f], [k], [t], [t̪], [s], and  
 733 [t̫]. These phones were then read as time series. Our selection  
 734 was limited to these voiced and voiceless consonants,  
 735 as we aimed to balance the ratio of voiced and voiceless  
 736 consonant records in these speech files. Additionally, some  
 737 consonants, such as [d] and [h], appeared difficult to classify  
 738 by our methods.

### 739 4.3 Deriving topological features from phonetic data

740 Prior to the extraction of topological features from a time  
 741 series, we first imbued this 1-dimensional time series with  
 742 a (Euclidean) topological structure through TDE. It is note-  
 743 worthy that this technique also applies to multi-dimensional  
 744 time series. The ambient space throughout this article is  
 745 always a Euclidean space. By establishing the topological  
 746 structure there, or more precisely, the distance matrices, we  
 747 subsequently calculated PH. We elaborate on the following  
 748 main steps. See Fig. 4e for the flow chart of this section.

#### 749 4.3.1 Data cleaning

750 This involved eliminating the initial and final segments of a  
 751 time series until the first point with an amplitude exceeding  
 752 0.03 occurred. This approach was aimed at mitigating the  
 753 impact of environmental noise at the beginning and end of a  
 754 phone. Any resulting series with fewer than 500 points will  
 755 be disregarded, as such series were considered insufficiently  
 756 long or to contain excessive environmental noise.

#### 757 4.3.2 Parameter selection for time-delay embedding

758 We selected suitable parameters for TDE to capture the the-  
 759oretically optimal MP of a given time series. The dimension  
 760 of the embedding was fixed to be 100. Our principle for  
 761 determining an appropriate dimension is that we want to  
 762 choose the embedded dimension to be large for a time series  
 763 of limited length. As discussed in Sec. 3 and cf. Sec. S.2.1, a  
 764 higher dimension results in a more accurate approximation.  
 765 This approach also aimed to enhance computational effi-  
 766 ciency and the occurrence of more prominent MP. Nonethe-  
 767 less, it is imperative to exercise caution when selecting the  
 768 dimension, as excessively large dimensions may lead to  
 769 empty point clouds and other uncontrollable factors.

770 With a proper dimension, we then computed the delay  
 771 for the embedding. According to Perea and Harer [61], in  
 772 the case of a periodic function, the optimal delays  $\tau$  can be  
 773 expressed as

$$\tau = m \cdot \frac{T}{d}$$

774 where  $T$  denotes the (minimal) period,  $d$  represents the  
 775 dimension of the embedding, and  $m$  is a positive integer.

776 Under these conditions, we could obtain the theoretically  
 777 optimal MP. The time series under consideration in our case  
 778 was far from periodic, however, so we used the first peak of  
 779 the ACL function to represent the period  $T$  and set  $m = 6$ ,  
 780 thus obtaining a relatively proper delay  $\tau$ . The common  
 781 choice of  $\tau$  is to let window size equal the (minimal) period.  
 782 However, in the case of a discrete time series, one often  
 783 obtains  $\tau = 0$  or  $\tau = 1$  in this way, since the dimension of  
 784 TDE is too large in comparison. Therefore, one strategy is to  
 785 increase  $m$  to get a relatively reasonable  $\tau$ . The performance  
 786 of delay obtained in this way is presented in Sec. 3.

787 Then  $\tau$  was rounded to the nearest integer (if it equals  
 788 0, take 1 instead). It was common that  $\tau \cdot d$  exceeded  
 789 the number of points in the series, resulting in an empty  
 790 embedding. In this case, we adopted  $\tau = |S|/d$ , where  
 791  $|S|$  denotes the number of points (i.e., the point capacity  
 792 of the time series), and then rounded it downwards. This  
 793 enabled us to obtain the appropriate delay for each time  
 794 series, thereby facilitating the attainment of significant MP  
 795 for the specified dimension.

796 Lastly, we let skip equal to 5. We chose this skip mainly  
 797 to reach a satisfactory computation time. The impact of the  
 798 skip parameter in TDE on MP and computation time is  
 799 expounded upon in Sec. S.3.1.

800 Once the parameters were set, the time series were  
 801 transformed into point clouds. If the number  $|P|$  of points in  
 802 a point cloud was less than 40, we excluded this time series  
 803 from further analysis, considering that there were too few  
 804 points to represent the original structure of the time series.  
 805 The problem of lacking points is also discussed in Sec. 3.

#### 806 4.3.3 Computing persistent homology

807 Using Ripser [70, 71], we could compute the PDs of the  
 808 point clouds in a fast and efficient way. We then extracted  
 809 MP from each 1-dimensional PD, using persistence birth  
 810 time and lifetime as two features of a time series. The  
 811 process of vectorising a PD presents a challenge due to the  
 812 indeterminate (and potentially large) number of intervals in  
 813 the barcode, coupled with the ambiguous information they  
 814 contain. This ambiguity arises from our lack of knowledge  
 815 about the types of information that can be derived from  
 816 different parts of the PD. Here we only extracted the MP  
 817 and corresponding birth time. This decision was informed  
 818 by our prior selection of an appropriate set of parameters,  
 819 which ensured that the MP reached its optimal.

## 820 5 DATA AND CODE AVAILABILITY

821 The data that support the findings of this study are openly  
 822 available in SpeechBox [67], ALLSTAR Corpus, L1-ENG  
 823 division at <https://speechbox.linguistics.northwestern.edu>.

824 The source code and supplementary materials for Top-  
 825 Cap can be accessed on the GitHub page at [https://github.com/AnnFeng233/TDA\\_Consonant\\_Recognition](https://github.com/AnnFeng233/TDA_Consonant_Recognition).

## REFERENCES

- [1] Gunnar Carlsson. "Topology and data". In: *Bulletin of The American Mathematical Society* 46 (Apr. 2009), pp. 255–308. DOI: 10.1090/S0273-0979-09-01249-X.
- [2] Ephy R. Love et al. "Topological convolutional layers for deep learning". In: *Journal of Machine Learning Research* 24.59 (2023), pp. 1–35.
- [3] Gunnar Carlsson and Rickard Brüel Gabrielsson. "Topological approaches to deep learning". In: *Topological Data Analysis: The Abel Symposium 2018*. Springer. 2020, pp. 119–146.
- [4] Ken W Grant, Brian E Walden, and Philip F Seitz. "Auditory-visual speech recognition by hearing-impaired subjects: Consonant recognition, sentence recognition, and auditory-visual integration". In: *The Journal of the Acoustical Society of America* 103.5 (1998), pp. 2677–2690. ISSN: 0001-4966.
- [5] Yichen Shen et al. "Deep learning with coherent nanophotonic circuits". In: *Nature Photonics* 11.7 (2017), pp. 441–446. ISSN: 1749-4893.
- [6] Eric W Healy et al. "Speech-cue transmission by an algorithm to increase consonant recognition in noise for hearing-impaired listeners". In: *The Journal of the Acoustical Society of America* 136.6 (2014), pp. 3325–3336. ISSN: 0001-4966.
- [7] Thierry Nazzi and Anne Cutler. "How consonants and vowels shape spoken-language recognition". In: *Annual Review of Linguistics* 5 (2019), pp. 25–47. ISSN: 2333-9683.
- [8] Dianne J Van Tasell et al. "Speech waveform envelope cues for consonant recognition". In: *The Journal of the Acoustical Society of America* 82.4 (1987), pp. 1152–1161. ISSN: 0001-4966.
- [9] DeLiang Wang and Guoning Hu. "Unvoiced speech segregation". In: *2006 IEEE International Conference on Acoustics Speech and Signal Processing Proceedings*. Vol. 5. 2006, pp. V–V. DOI: 10.1109/ICASSP.2006.1661435.
- [10] Philip Weber et al. "Consonant recognition with continuous-state hidden Markov models and perceptually-motivated features". In: *Sixteenth Annual Conference of the International Speech Communication Association*. 2015.
- [11] Gunnar Carlsson et al. "Persistence barcodes for shapes". In: *International Journal of Shape Modeling* 11.02 (2005), pp. 149–187. DOI: 10.1142/s0218654305000761.
- [12] Oleksandr Balabanov and Mats Granath. "Unsupervised learning using topological data augmentation". In: *Physical Review Research* 2.1 (2020), p. 013354.
- [13] Azadeh Hadadi et al. "Prediction of cybersickness in virtual environments using topological data analysis and machine learning". In: *Frontiers in Virtual Reality* 3 (2022), p. 973236. ISSN: 2673-4192.
- [14] Firas A. Khasawneh, Elizabeth Munch, and Jose A. Perea. "Chatter classification in turning using machine learning and topological data analysis". In: *IFAC-PapersOnLine* 51.14 (2018), pp. 195–200. ISSN: 2405-8963. DOI: 10.1016/j.ifacol.2018.07.222.
- [15] Daniel Leykam and Dimitris G. Angelakis. "Topological data analysis and machine learning". In: *Advances in Physics: X* 8.1 (2023). ISSN: 2374-6149. DOI: 10.1080/23746149.2023.2202331.
- [16] Grzegorz Muszynski et al. "Topological data analysis and machine learning for recognizing atmospheric river patterns in large climate datasets". In: *Geoscientific Model Development* 12.2 (2019), pp. 613–628. ISSN: 1991-9603. DOI: 10.5194/gmd-12-613-2019.
- [17] Frédéric Chazal and Bertrand Michel. "An introduction to topological data analysis: Fundamental and practical aspects for data scientists". In: *Frontiers in Artificial Intelligence* 4 (2021), p. 108. ISSN: 2624-8212.
- [18] Aras Asaad and Sabah Jassim. "Topological data analysis for image tampering detection". In: *Digital Forensics and Watermarking: 16th International Workshop, IWDW 2017, Magdeburg, Germany, August 23–25, 2017, Proceedings* 16. Springer. 2017, pp. 136–146.
- [19] Lander Ver Hoef et al. "A primer on topological data analysis to support image analysis tasks in environmental science". In: *Artificial Intelligence for the Earth Systems* 2.1 (2023), e220039.
- [20] Gunnar Carlsson et al. "On the local behavior of spaces of natural images". In: *International Journal of Computer Vision* 76 (Jan. 2008), pp. 1–12. DOI: 10.1007/s11263-007-0056-x.
- [21] Sebastian Zeng et al. "Topological attention for time series forecasting". In: *Advances in Neural Information Processing Systems* 34 (2021), pp. 24871–24882.
- [22] Yuhei Umeda. "Time series classification via topological data analysis". In: *Information and Media Technologies* 12 (2017), pp. 228–239. ISSN: 1881-0896.
- [23] Manish Saggar et al. "Towards a new approach to reveal dynamical organization of the brain using topological data analysis". In: *Nature Communications* 9.1 (2018), p. 1399. ISSN: 2041-1723. DOI: 10.1038/s41467-018-03664-4.
- [24] Jessica L Nielson et al. "Uncovering precision phenotype-biomarker associations in traumatic brain injury using topological data analysis". In: *PloS One* 12.3 (2017), e0169490. ISSN: 1932-6203.
- [25] Tamal K Dey and Sayan Mandal. "Protein classification with improved topological data analysis". In: *18th International Workshop on Algorithms in Bioinformatics (WABI 2018)*. Schloss Dagstuhl-Leibniz-Zentrum fuer Informatik. 2018.
- [26] Alessio Martino, Antonello Rizzi, and Fabio Massimo Frattale Mascioli. "Supervised approaches for protein function prediction by topological data analysis". In: *2018 International Joint Conference on Neural Networks (IJCNN)*. IEEE. 2018, pp. 1–8.
- [27] Kenneth Brown and Kevin Knudson. "Nonlinear statistics of human speech data". In: *International Journal of Bifurcation and Chaos* 19 (July 2009), pp. 2307–2319. DOI: 10.1142/S0218127409024086.
- [28] Sergio Barbarossa and Stefania Sardellitti. "Topological signal processing over simplicial complexes". In: *IEEE Transactions on Signal Processing* 68 (2020), pp. 2992–3007.

- [29] Eduard Tulchinskii et al. "Topological data analysis for speech processing". In: *Proc. Interspeech 2023*, pp. 311–315. DOI: 10.21437/Interspeech.2023-1861.
- [30] Deli Chen et al. "Measuring and relieving the over-smoothing problem for graph neural networks from the topological view". In: *Proceedings of the AAAI Conference on Artificial Intelligence*. Vol. 34. 2020, pp. 3438–3445.
- [31] Woong Bae, Jaejun Yoo, and Jong Chul Ye. "Beyond deep residual learning for image restoration: Persistent homology-guided manifold simplification". In: *Proceedings of the IEEE Conference on Computer Vision and Pattern Recognition Workshops*. 2017, pp. 145–153.
- [32] Christoph Hofer et al. "Deep learning with topological signatures". In: *Advances in Neural Information Processing Systems* 30 (2017).
- [33] Emilie Gerardin et al. "Multidimensional classification of hippocampal shape features discriminates Alzheimer's disease and mild cognitive impairment from normal aging". In: *Neuroimage* 47.4 (2009), pp. 1476–1486. ISSN: 1053-8119.
- [34] Mingqiang Yang, Kidiyo Kpalma, and Joseph Ronzin. "A survey of shape feature extraction techniques". In: *Pattern Recognition* 15.7 (2008), pp. 43–90.
- [35] Zenggang Xiong et al. "Research on image retrieval algorithm based on combination of color and shape features". In: *Journal of Signal Processing Systems* 93 (2021), pp. 139–146. ISSN: 1939-8018.
- [36] Dengsheng Zhang and Guojun Lu. "Review of shape representation and description techniques". In: *Pattern Recognition* 37.1 (2004), pp. 1–19. ISSN: 0031-3203. DOI: 10.1016/j.patcog.2003.07.008.
- [37] John Lee. *Introduction to topological manifolds*. Vol. 202. Springer Science & Business Media, 2010. ISBN: 1441979409.
- [38] Allen Hatcher. *Algebraic topology*. Cambridge: Cambridge University Press, 2002.
- [39] Afra Zomorodian and Gunnar Carlsson. "Computing persistent homology". In: *Discrete & Computational Geometry* 33.2 (2005), pp. 249–274. ISSN: 1432-0444. DOI: 10.1007/s00454-004-1146-y.
- [40] Herbert Edelsbrunner and John Harer. "Persistent homology – a survey". In: *Contemporary Mathematics* 453.26 (2008), pp. 257–282.
- [41] Robert Ghrist. "Barcodes: The persistent topology of data". In: *Bulletin of the American Mathematical Society* 45.1 (2008), pp. 61–75. ISSN: 0273-0979.
- [42] David Cohen-Steiner, Herbert Edelsbrunner, and John Harer. "Stability of persistence diagrams". In: *Proceedings of the Twenty-First Annual Symposium on Computational geometry*. 2005, pp. 263–271.
- [43] Charu C Aggarwal, Alexander Hinneburg, and Daniel A Keim. "On the surprising behavior of distance metrics in high dimensional space". In: *Database Theory—ICDT 2001: 8th International Conference London, UK, January 4–6, 2001 Proceedings* 8. Springer, 2001, pp. 420–434.
- [44] Vladislav Polianskii and Florian T. Pokorný. "Voronoi graph traversal in high dimensions with applications to topological data analysis and piecewise linear interpolation". In: *Proceedings of the 26th ACM SIGKDD International Conference on Knowledge Discovery & Data Mining*. KDD '20. Virtual Event, CA, USA: Association for Computing Machinery, 2020, pp. 2154–2164. ISBN: 9781450379984. DOI: 10.1145/3394486.3403266.
- [45] Matthew B Kennel, Reggie Brown, and Henry DI Abarbanel. "Determining embedding dimension for phase-space reconstruction using a geometrical construction". In: *Physical Review A* 45.6 (1992), p. 3403.
- [46] Baihan Lin. "Topological data analysis in time series: Temporal filtration and application to single-cell genomics". In: *Algorithms* 15.10 (2022), p. 371. ISSN: 1999-4893.
- [47] Saba Emrani, Thanos Gentimis, and Hamid Krim. "Persistent homology of delay embeddings and its application to wheeze detection". In: *IEEE Signal Processing Letters* 21.4 (2014), pp. 459–463. ISSN: 1070-9908.
- [48] Cássio MM Pereira and Rodrigo F de Mello. "Persistent homology for time series and spatial data clustering". In: *Expert Systems with Applications* 42.15-16 (2015), pp. 6026–6038. ISSN: 0957-4174.
- [49] Firas A Khasawneh and Elizabeth Munch. "Chatter detection in turning using persistent homology". In: *Mechanical Systems and Signal Processing* 70 (2016), pp. 527–541. ISSN: 0888-3270.
- [50] Lee M Seversky, Shelby Davis, and Matthew Berger. "On time-series topological data analysis: New data and opportunities". In: *Proceedings of the IEEE Conference on Computer Vision and Pattern Recognition Workshops*. 2016, pp. 59–67.
- [51] Marian Gidea and Yuri Katz. "Topological data analysis of financial time series: Landscapes of crashes". In: *Physica A: Statistical Mechanics and its Applications* 491 (2018), pp. 820–834. ISSN: 0378-4371.
- [52] Richard Bellman. "Dynamic programming". In: *Science* 153.3731 (1966), pp. 34–37.
- [53] Afra Zomorodian and Gunnar Carlsson. "Computing persistent homology". In: *Discrete & Computational Geometry* 33.2 (Feb. 2005), pp. 249–274. ISSN: 1432-0444. DOI: 10.1007/s00454-004-1146-y.
- [54] Nikola Milosavljević, Dmitriy Morozov, and Primoz Skraba. "Zigzag persistent homology in matrix multiplication time". In: *Proceedings of the Twenty-Seventh Annual Symposium on Computational Geometry*. 2011, pp. 216–225.
- [55] Peter Bubenik. "Statistical topological data analysis using persistence landscapes". In: *Journal of Machine Learning Research* 16.1 (2015), pp. 77–102.
- [56] Henry Adams et al. "Persistence images: A stable vector representation of persistent homology". In: *Journal of Machine Learning Research* 18 (2017).
- [57] D. Ali et al. "A survey of vectorization methods in topological data analysis". In: *IEEE Transactions on Pattern Analysis and Machine Intelligence* (2023), pp. 1–14. ISSN: 1939-3539. DOI: 10.1109/TPAMI.2023.3308391.
- [58] James D Hamilton. *Time series analysis*. Princeton University Press, 2020.
- [59] Yu-Min Chung et al. "A persistent homology approach to heart rate variability analysis with an

- 1069 application to sleep-wake classification". In: *Frontiers*  
 1070 in *Physiology* 12 (2021), p. 637684. ISSN: 1664-042X.  
 1071 [60] Jose A Perea. "Topological time series analysis".  
 1072 In: *Notices of the American Mathematical Society* 66.5  
 1073 (2019), pp. 686–694.  
 1074 [61] Jose A. Perea and John Harer. "Sliding windows and  
 1075 persistence: An application of topological methods  
 1076 to signal analysis". In: *Foundations of Computational*  
 1077 *Mathematics* 15.3 (June 2015), pp. 799–838. ISSN: 1615-  
 1078 3383. DOI: 10.1007/s10208-014-9206-z.  
 1079 [62] Jose Perea et al. "SW1PerS: Sliding windows and 1-  
 1080 persistence scoring; discovering periodicity in gene  
 1081 expression time series data". In: *BMC bioinformatics*  
 1082 16 (Aug. 2015), p. 257. DOI: 10.1186/s12859-015-  
 1083 0645-6.  
 1084 [63] Christopher Tralie and Jose Perea. "(Quasi) periodicity  
 1085 quantification in video data, using topology". In:  
 1086 *SIAM Journal on Imaging Sciences* 11 (Apr. 2017). DOI:  
 1087 10.1137/17M1150736.  
 1088 [64] Hitesh Gakhar and Jose A. Perea. "Sliding window  
 1089 persistence of quasiperiodic functions". In: *Journal of*  
 1090 *Applied and Computational Topology* (2023). DOI: 10.  
 1091 1007/s41468-023-00136-7.  
 1092 [65] NOAA. *Climate at a glance: National time series*. Na-  
 1093 tional Centers for Environmental Information, re-  
 1094 trievalled 28th January 2023 from <https://www.citedrive.com/overleaf>.  
 1095 [66] Holger Kantz and Thomas Schreiber. *Nonlinear time*  
 1096 *series analysis*. Vol. 7. Cambridge University Press,  
 1097 2004.  
 1098 [67] A. R. Bradlow. SpeechBox, retrieved from <https://speechbox.linguistics.northwestern.edu>.  
 1099 [68] Michael McAuliffe et al. "Montreal Forced Aligner:  
 1100 Trainable text-speech alignment using Kaldi". In:  
 1101 *Proc. Interspeech 2017*, pp. 498–502. DOI: 10.21437/  
 1102 Interspeech.2017-1386.  
 1103 [69] Paul Boersma and David Weenink. *Praat: Doing*  
 1104 *phonetics by computer*. Version 6.3.09, retrieved 2nd  
 1105 March 2023 from <http://www.praat.org/>. 2023.  
 1106 [70] Christopher Tralie, Nathaniel Saul, and Rann Bar-On.  
 1107 "Ripser.py: A Lean persistent homology library for  
 1108 Python". In: *The Journal of Open Source Software* 3.29  
 1109 (Sept. 2018), p. 925. DOI: 10.21105/joss.00925.  
 1110 [71] Ulrich Bauer. "Ripser: Efficient computation of  
 1111 Vietoris-Rips persistence barcodes". In: *Journal of Ap-  
 1112 plied and Computational Topology* 5.3 (2021), pp. 391–  
 1113 423. DOI: 10.1007/s41468-021-00071-5.  
 1114  
 1115
- 12371069 and the Guangdong Provincial Key Laboratory of  
 1128 Interdisciplinary Research and Application for Data Science. 1129

## AUTHOR INFORMATION

### Authors and Affiliations

1130 **Department of Mathematics, Southern University of Sci-  
 1131 ence and Technology, Shenzhen, China** 1132  
 1133 Pingyaо Feng, Siheng Yi, Qingrui Qu, Zhiwang Yu, Yifei  
 1134 Zhu 1135

### Contributions

1136 Y.Z. planned the project. P.F. and S.Y. constructed the the-  
 1137 oretical framework. P.F. designed the sample, built the  
 1138 algorithms, and analysed the data. S.Y. assisted with the  
 1139 algorithms. P.F., S.Y., Q.Q., Z.Y., and Y.Z. wrote the paper  
 1140 and contributed to the discussion. 1141

### Corresponding authors

1142 Correspondence to Pingyaо Feng or Yifei Zhu. 1143

## ACKNOWLEDGEMENTS

1116 The authors would like to thank Meng Yu for his invaluable  
 1117 mentorship on audio and speech signal processing, on neu-  
 1118 ral networks and deep learning, as well as for his comments  
 1119 and suggestions on an earlier draft of this manuscript.  
 1120 The authors would also like to thank Andrew Blumberg,  
 1121 Fangyi Chen, Haibao Duan, Houhong Fan, Fuquan Fang,  
 1122 Wenfei Jin, Fengchun Lei, Yanlin Li, Andy Luchuan Liu,  
 1123 Tao Luo, Zhi Lü, Jianxin Pan, Jie Wu, Kelin Xia, Jiang  
 1124 Yang, Jin Zhang and Zhen Zhang for helpful discussions  
 1125 and encouragement. This work was partly supported by  
 1126 the National Natural Science Foundation of China grant  
 1127

## 1144 SUPPLEMENTARY INFORMATION

### 1145 S.1 Generalities on phonetic data

1146 As a research field of linguistics, phonetics studies the  
 1147 production as well as the classification of human speech  
 1148 sounds from the world's languages. In phonetics, a *phone* is  
 1149 the smallest basic unit of human speech sounds. It is a short  
 1150 speech segment possessing distinct physical or perceptual  
 1151 properties. Phones are generally classified into two principal  
 1152 categories: vowels and consonants. A *vowel* is defined as a  
 1153 speech sound pronounced by an open vocal tract with no  
 1154 significant build-up of air pressure at any point above the  
 1155 glottis, and at least making some airflow escape through  
 1156 the mouth. In contrast, a *consonant* is a speech sound that  
 1157 is articulated with a complete or partial closure of the vocal  
 1158 tract and usually forces air through a narrow channel in  
 1159 one's mouth or nose.

1160 Unlike vowels which must be pronounced by vibrated  
 1161 vocal cords, consonants can be further categorised into two  
 1162 classes according to whether the vocal cords vibrate or not  
 1163 during articulation. If the vocal cords vibrate, the consonant  
 1164 is known as a *voiced* consonant. Otherwise, the consonant is  
 1165 *voiceless*. Since vocal cord vibration can produce a stable per-  
 1166 iodical signal of air pressure, voiced consonants tend to have  
 1167 more periodic components than voiceless consonants, which  
 1168 can in turn be detected by PH as topological characteristics  
 1169 from phonetic time series data.

1170 Indeed, one of the more heuristic motivations for our re-  
 1171 search project is to reexamine (and even revise) the linguistic  
 1172 classifications of phones through the mathematical lens of  
 1173 topological patterns and shape of speech data, analogous  
 1174 to Carlsson and his collaborators' seminal work [S1] on the  
 1175 distribution of image data (cf. Fig. S1).

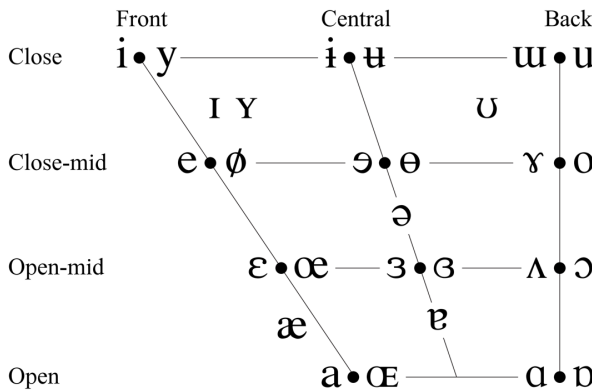


Fig. S1: A charted "distribution space" of vowels created by linguists [S2]. The vertical axis of the chart denotes vowel height. Vowels pronounced with the tongue lowered are located at the bottom and those raised are at the top. The horizontal axis of this chart denotes vowel backness. Vowels with the tongue moved towards the front of the mouth are in the left of the chart, while those with to the back are placed in the right. The last parameter is whether the lips are rounded. At each given spot, vowels on the right and left are rounded and unrounded, respectively.

## 1176 S.2 Mathematical generalities of the TDE–PH approach 1177 to time series data

### 1178 S.2.1 Time-delay embedding

1179 Time-delay embedding (TDE) is also known as sliding win-  
 1180 dow embedding, delay embedding, and delay coordinate  
 1181 embedding. For simplicity, we focus on 1-dimensional time  
 1182 series. TDE of a real-valued function  $f: \mathbb{R} \rightarrow \mathbb{R}$ , with  
 1183 parameters positive integer  $d$  and positive real number  $\tau$ ,  
 1184 is defined to be the vector-valued function  
 1185

$$1186 SW_{d,\tau} f: \mathbb{R} \rightarrow \mathbb{R}^d$$

$$1187 t \mapsto (f(t), f(t + \tau), \dots, f(t + (d - 1)\tau))$$

1188 Here,  $d$  is the *dimension* of the target space for the embed-  
 1189 ding,  $\tau$  is the *delay*, and their product  $d \cdot \tau$  is called the  
 1190 *window size*. According to the Manifold Hypothesis, a time  
 1191 series lies on a manifold. The method then reconstructs  
 1192 this topological space from the input time series, when  
 1193  $d$  is at least twice the dimension of the latent manifold  
 1194  $M$ . Given a trajectory  $\gamma: \mathbb{R} \rightarrow M$  whose image is dense  
 1195 in  $M$ , the embedding property holds for the time series  
 1196  $f(t_n)$  (generically, in a technical sense we omit here) via an  
 1197 "observation" function  $G: M \rightarrow \mathbb{R}$ , i.e.,  $f(t_n) = G(\gamma(t_n))$ .

1198 In [S3, Sec. 5], Perea and Harer established that the  $N$ -  
 1199 truncated Fourier series expansion

$$1200 S_N f(t) = \sum_{n=0}^N a_k \cos(kt) + b_k \sin(kt)$$

1201 of a periodic time series  $f$  can be reconstructed into a circle  
 1202 when  $d \geq 2N$ , i.e.,

$$1203 SW_{d,\tau} f(\mathbb{R}) \cong \mathbb{S}^1$$

1204 Moreover, let  $L$  be a constant such that

$$1205 f\left(t + \frac{2\pi}{L}\right) = f(t)$$

1206 Then the 1-dimensional MP of the resulting point cloud  
 1207 is the largest when the window size  $d \cdot \tau$  is integrally  
 1208 proportional to  $2\pi/L$ , i.e.,

$$1209 d \cdot \tau = m \frac{2\pi}{L}$$

1210 for a positive integer  $m$ . Intuitively, an increase in the  
 1211 dimension of TDE results in a better approximation when  
 1212 truncating the Fourier series, and the MP of the point cloud  
 1213 becomes the most significant when the window size equals  
 1214 a period.

1215 This methodology also proves particularly advantageous  
 1216 in scenarios where the system under investigation exhibits  
 1217 nonlinear dynamics, precluding straightforward analysis of  
 1218 the time series data. Via a suitable embedding, the inherent  
 1219 geometric configuration of the system emerges, enabling  
 1220 deeper comprehension and refined analysis.

### 1221 S.2.2 Persistent homology

1222 Topology is a subject area that studies the properties of  
 1223 geometric objects that remain unchanged under continuous  
 1224 transformations or smooth perturbations. It focuses on the  
 1225 intrinsic features of a space that regardless of its rigid shape  
 1226 or size. Algebraic topology (AT) provides a quantitative  
 1227 description of these topological properties.

A simplicial complex (and its numerous variants and analogues) is a powerful tool in AT which enables us to represent a topological space using discrete data. Unlike the original space, which can be challenging to compute and analyse, a simplicial complex provides a combinatorial description that is much more amenable to computation. We can use algebraic techniques to study the properties of a simplicial complex, such as its homology and cohomology groups, which encode and reveal information about the topology of the underlying space.

Formally, a *simplicial complex* with vertices in a set  $V$  is a collection  $K$  of nonempty finite subsets  $\sigma \subset V$  such that any nonempty subset  $\tau$  of  $\sigma$  always implies  $\tau \in K$  (called a *face* of  $\sigma$ ) and that  $\sigma$  intersecting  $\sigma'$  implies their intersection  $\sigma \cap \sigma' \in K$ . A set  $\sigma \in K$  with  $(i+1)$  elements is called an *i-simplex* of the simplicial complex  $K$ . For instance, consider  $\mathbb{S}^1 \vee \mathbb{S}^2$ , a circle kissing a sphere at a single point, as a topology space. It can be approximated by the simplicial complex  $K$  with 6 vertices  $a, b, c, d, e, f$ . This simplicial complex can be enumerated as

$$\begin{aligned} K = & \{\{a\}, \{b\}, \{c\}, \{d\}, \{e\}, \{f\}, \\ & \{a, b\}, \{a, c\}, \{b, c\}, \{c, d\}, \{c, f\}, \{d, f\}, \{c, e\}, \\ & \{d, e\}, \{f, e\}, \\ & \{c, d, f\}, \{c, e, f\}, \{c, d, e\}, \{d, e, f\}\} \end{aligned}$$

which is a combinatorial avatar for  $\mathbb{S}^1 \vee \mathbb{S}^2$  via a “triangulation” operation on the latter. See Fig. S2.

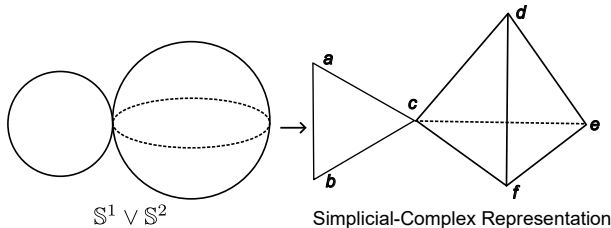


Fig. S2: From a topological space to its triangulation.

Given a simplicial complex  $K$ , let  $p$  be a prime number and  $\mathbb{F}_p$  be the finite field with  $p$  elements. Define  $C_i(K; \mathbb{F}_p)$  to be the  $\mathbb{F}_p$ -vector space with basis the set of  $i$ -simplices in  $K$ . To keep track of the order of vertices within a simplex, we use the alternative notation with square brackets in the following. If  $\sigma = [v_0, v_1, \dots, v_i]$  is an  $i$ -simplex, define the *boundary* of  $\sigma$ , denoted by  $\partial\sigma$ , to be the alternating sum of the  $(i-1)$ -dimensional faces of  $\sigma$  given by

$$\partial\sigma := \sum_{k=0}^i (-1)^k [v_0, \dots, \hat{v}_k, \dots, v_i]$$

where  $[v_0, \dots, \hat{v}_k, \dots, v_i]$  is the  $k$ -th  $(i-1)$ -dimensional face of  $\sigma$  missing the vertex  $v_k$ . We can extend  $\partial$  to  $C_i(K; \mathbb{F}_p)$  as an  $\mathbb{F}_p$ -linear operator so that  $\partial: C_i(K; \mathbb{F}_p) \rightarrow C_{i-1}(K; \mathbb{F}_p)$ . The composition of boundary operators satisfies  $\partial \circ \partial = 0$ . The elements in  $C_i(K; \mathbb{F}_p)$  with boundary 0 are called *i-cycles*. They form a subspace of  $C_i(K; \mathbb{F}_p)$ , denoted by  $Z_i(K; \mathbb{F}_p)$ . The elements in  $C_i(K; \mathbb{F}_p)$  that are the images of elements of  $C_{i+1}(K; \mathbb{F}_p)$  under  $\partial$  are called *i-boundaries*.

They form a subspace too, denoted by  $B_i(K; \mathbb{F}_p)$ . It follows from  $\partial \circ \partial = 0$  that

$$B_i(K; \mathbb{F}_p) \subset Z_i(K; \mathbb{F}_p)$$

Then define the quotient space

$$H_i(K; \mathbb{F}_p) := Z_i(K; \mathbb{F}_p) / B_i(K; \mathbb{F}_p)$$

to be the *i-th homology group* of  $K$  with  $\mathbb{F}_p$ -coefficients. We call  $\dim(H_i(K; \mathbb{F}_p))$  the *i-th Betti number*, denoted by  $\beta_i(K)$ , which counts the number of  $i$ -dimensional holes in the corresponding topological space. As such, these homology groups are also called the homology groups of the space (it can be shown that they are independent of the particular ways in which the space is triangulated). For example, the Betti numbers of  $\mathbb{S}^1 \vee \mathbb{S}^2$  from above are  $\beta_1 = 1$ ,  $\beta_2 = 1$ , and  $\beta_i = 0$  when  $i \geq 3$ .

The usefulness of these invariants, besides their computability (essentially Gaussian elimination in linear algebra), lies in their tractability along deformations. Given two simplicial complexes  $K$  and  $L$ , a simplicial map  $f: K \rightarrow L$  (that preserves the simplicial structure) induces an  $\mathbb{F}_p$ -linear map  $H_i(f; \mathbb{F}_p): H_i(K; \mathbb{F}_p) \rightarrow H_i(L; \mathbb{F}_p)$ . Thus, if two spaces are topologically equivalent (in fact, “homotopy equivalent” suffices), their homology groups must be isomorphic and the Betti numbers match up.

Let  $(X, d)$  be a finite point cloud with metric  $d$ . Define a family of simplicial complexes, called *Rips complexes*, by

$$R_\epsilon(X) := \{\sigma \subset X \mid d(x, x') \leq \epsilon \text{ for all } x, x' \in \sigma\}$$

The family

$$\mathcal{R}(X) := \{R_\epsilon(X)\}_{\epsilon \geq 0}$$

is known as the *Rips filtration* of  $X$ . Clearly, if  $\epsilon_1 \leq \epsilon_2$ , then  $R_{\epsilon_1}(X) \hookrightarrow R_{\epsilon_2}(X)$ . Thus, for each  $i$  we obtain a sequence

$$\begin{aligned} H_i(R_{\epsilon_0}(X); \mathbb{F}_p) &\rightarrow H_i(R_{\epsilon_1}(X); \mathbb{F}_p) \rightarrow \dots \\ &\rightarrow H_i(R_{\epsilon_m}(X); \mathbb{F}_p) \end{aligned}$$

where  $0 = \epsilon_0 < \epsilon_1 < \dots < \epsilon_m < \infty$ . As  $\epsilon$  varies, the topological features in the simplicial complexes  $R_\epsilon(X)$  vary, resulting in the emergence and disappearance of holes.

Given the values of  $\epsilon$ , record the instances of emergence and disappearance of holes, which correspond to cycle classes in the homology groups along the above sequence. Each class has a descriptor  $(b, d) \in \mathbb{R}^2$ , where  $b$  represents the *birth time*,  $d$  represents the *death time*, and  $b - d$  represents the *lifetime* of the holes. In this way, we obtain a multiset

$$\{(b_j, d_j)\}_{j \in J} =: \text{dgm}_i(\mathcal{R}(X))$$

which encodes the “persistence” of topological features of  $X$ . This multiset can be represented as a multiset of points in the 2-dimensional coordinate system called a *persistence diagram* for the *i-th PH* or as an array of interval segments called a *persistence barcode*. In particular, we use *maximal persistence* to refer to the maximal lifetime among all the points in a persistence diagram.

dimension = 10 desired delay = 40			dimension = 50 desired delay = 8			dimension = 100 desired delay = 4		
delay	skip	MP	delay	skip	MP	delay	skip	MP
1	1	0.0610	1	1	0.2834	1	1	0.4270
10	1	0.1299	3	1	0.3021	2	1	0.4337
20	1	0.1312	4	1	0.3054	2	5	0.4146
30	1	0.1281	5	1	0.3058	3	1	0.4357
39	1	0.1229	6	1	0.3042	3	5	0.4120
39	5	0.1134	7	1	0.3052	4	1	0.4381
40	1	0.1290	7	5	0.2886	4	5	0.4139
40	5	0.1195	8	1	0.3093	5	1	0.4375
41	1	0.1200	8	5	0.2928	5	5	0.4105
41	5	0.1153	9	1	0.3091	6	1	0.4347
45	1	0.0940	9	5	0.2913	6	5	0.4114
50	1	0.1226	10	1	0.3069	7	1	0.4380
60	1	0.1315	15	1	0.3070	8	1	0.4378
94	1	empty	18	1	empty	9	1	empty

Tab. S1: MP for choices of dimension, delay, and skip in TDE. The desired delay is computed by the algorithm in Sec. 4 of Methods. Empty in MP means the delay is too large to obtain point-cloud data.

### S.3 More specifics on parameter selection with TopCap

#### S.3.1 Skip, maximal persistence, and persistence execution time

Computation time assumes a critical role when processing a substantial volume of data. In this context, the parameter skip in TDE is considered, as it significantly influences the number of points within the point clouds, thereby directly impacting the number of simplices during persistent filtration and thus the computation time for PD. In this subsection, we demonstrate that an appropriate increment in the skip parameter can markedly reduce computation time. However, it is noteworthy that MP exhibits resilience to an increase in skip to a certain extent. Consequently, in this case, it is feasible to augment skip in TDE to expedite the computation of PD. For details on the complexity of computing persistent homology, the interested reader may refer to Zomorodian and Carlsson [S4, Sec. 4.3] as well as Edelsbrunner et al. [S5, Sec. 4].

Using an example of a sound record of the voiced consonant [m], we elucidate the relationship between skip, computation duration, and size of the resulting point clouds obtained via TDE in Fig. 6d. Computation duration is measured each time after restarting the Jupyter notebook, on Dell Precision 3581, with CPU Intel® Core™ i7-13800H of basic frequency 2.50 GHz and 14 cores. Computation time means the time for executing the code `ripser(Points,maxdim=1)`. As depicted in Fig. 6d, a substantial reduction in computation time is observed with an increase in the skip parameter. In contrast, our computation's output MP appears stable.

#### S.3.2 Multiple dependency of maximal persistence

As mentioned in the main text, there are three crucial parameters in TDE, namely,  $d$ ,  $\tau$ , and skip. In this subsection, we present a table that delineates the topological descriptor MP in relation to these from TopCap.

The experiment is executed on a record of the voiced consonant [ŋ], which comprises 887 sampled points as the length of this time series. Theoretically, given a periodic function, one obtains the optimal MP of the function in a fixed dimension under the condition that the TDE window size (i.e., the product of dimension and delay) equals a period (cf. Sec. S.2.1). However, the phonetic time series

that we typically handle deviate far from being periodic. Despite our approach to calculating the period of time series by ACL functions, we cannot assure that the (theoretically derived) desired delay will indeed yield the optimal MP of a time series in general. Nevertheless, this desired delay usually gives relatively good MP. For instance, as illustrated in Tab. S1, when the dimension is 10, the desired delay is 40. This corresponds to an MP of 0.1290, which is marginally lower than the MP of 0.1315 achieved at a delay of 60. However, as the dimension rises, the point clouds from TDE become more regular. It becomes increasingly probable that at the desired delay, one can indeed obtain the optimal MP of the time series. For example, when the dimension is either 50 or 100, the MP of the time series is achieved at the desired delay. This provides additional justification for preferring higher dimensions: The table reveals that an augmentation in dimension may lead to a more substantial enhancement in the MP of a time series than simply tuning delay.

### S.4 Review and outlook on topology-enhanced machine learning

Here we present a general review of literature on the topics (1) TDA and its applications, which encompasses genesis of the subject, recommended resources, and practical applications; (2) vectorisation of PH, wherein we summarize topological methods geared towards machine learning.

#### S.4.1 Topological data analysis and its applications

The evolution of TDA is relatively nascent when juxtaposed with other enduring fields, and its applications are still somewhat delimited. The genesis of the concept of invariants of filtered complexes can be traced back to Baranikov in 1994, which are nowadays referred to as PD/PB (persistence diagram/barcode) [S6]. These invariants were conceived with the objective of quantifying some specific critical point within some ambit of an extension of function. In 1999, Robins pioneered the concept of *persistent Betti numbers* of inverse systems and underscored their stability in Hausdorff distance [S7].

The modern incarnation of persistent homology was established in the first decade of the 21st century. Zomorodian, under the tutelage of Edelsbrunner, completed his doctoral

thesis in 2001, wherein he employed persistence to distinguish between topological noise and inherent features of a space [S8]. After that, the term *persistent homology group* first appeared in the work by Edelsbrunner et al. in 2002 [S9]. This seminal work formalised topological methodologies to chronicle the evolution of an expanding complex originating from a point set in Euclidean 3-space, a process they termed as topological simplification. The expansion process is recognised as filtration. They classified topological modifications based on the lifetime of topological features during filtration and proposed an algorithm to compute this simplification process. Subsequently, in 2005, Carlsson et al. applied persistent homology to generate a barcode as a shape descriptor [S10]. Their methodology was able to distinguish between shapes with varying degrees of “sharp” features, such as corners. In the same year, Zomorodian and Carlsson presented an algebraic interpretation of persistent homology and developed a natural algorithm for computing persistent homology of spaces in any dimension over any field [S11]. Cohen-Steiner et al. considered the stability property of persistence algorithm [S12]. Robustness is measured by the bottleneck distance between persistence diagrams.

In 2008, Carlsson, Singh, and Sexton founded Ayasdi, a company that combines mathematics and finance to truly put theory into practice. The inception of TDA may be complex, as it originates from some pure mathematical fields such as Morse theory and PH. However, the underlying principle remains steadfast: to identify topological features that can quantify the shape of the data to certain degrees, which is robust against noise and perturbations.

An abundance of materials is available that offer a thorough understanding of TDA for both specialists and general audience. In 2009, Carlsson wrote an extensive survey on the applications of geometry and topology to the analysis of various types of data [S13]. This work introduced topics such as the characteristics of topological methods, persistence, and clusters. A recent publication by Carlsson and Vejdemo-Johansson discussed practical case studies of topological methods, such as their applications to image data and time series [S14]. For nonspecialists seeking to delve into TDA, the introductory article [S15] by Chazal and Michel may be more accessible. It provides explicit explanations and hands-on guidance on both the theoretical and practical aspects of the subject.

Several software tools assist researchers in building case studies on data. The GUDHI library [S16], an open-source C++ library with a Python interface, includes a comprehensive set of tools involving different complexes and vectorisation tools. Ripser [S17], also a C++ library with a Python binding, surpasses GUDHI in computing Vietoris–Rips PD/PB, especially when high-dimensional cases or large quantities of PD/PB are present. TTK [S18] is both a library and software designed for topological analysis with a focus on scientific visualisation. Other standard libraries include Dionysus, PHAT, DIPHA, and Giotto<sup>2</sup>. Additionally,

an R interface named TDA [S19] is available for the libraries GUDHI, Dionysus, and PHAT.

The recent proliferation of TDA has established it as an effective instrument in numerous studies. Owing to the characteristics of topological methods [S13], a multitude of applications have been discovered, particularly in the realm of recognition. In the field of biomedicine, Nicolau et al. utilised the topological method Mapper [S20] to analyse transcriptional data related to breast cancer [S21]. This method is used due to its high performance in shape recognition in high dimensions. The book [S22] authored by Rabadán and Blumberg provides an introduction to TDA techniques and their specific applications in biology, encompassing topics such as evolutionary processes and cancer genomics.

In signal processing, Emrani et al. introduced a topological approach for the analysis of breathing sound signals for the detection of wheezing, which can distinguish abnormal wheeze signals from normal breathing signals due to the periodic patterns within wheezing [S23]. Robinson’s monograph [S24] offers a systematic exploration of the intersection between topology and signal processing.

In the context of deep learning, Bae et al. proposed a PH-based deep residual learning algorithm for image restoration tasks [S25]. Hofer et al. incorporated topological signatures into deep neural networks to learn unusual structures that are typically challenging for most machine learning techniques [S26]. More recently, having extracted statistical features of images and videos through topological means, Love et al. input these features to the kernel of convolutional layers [S27, S1]. In their case, manifolds in relation to the natural-image space are used to parametrise image filters, which also parametrise slices in layers of neural networks. These signify a new phase of development for the subject.

For complex networks, an early application of PH on sensor networks is presented in the work [S28] by de Silva and Ghrist. They applied topological methods to graphs representing the distance estimation between nodes and a proximity sensor. Subsequently, Horak et al. discussed PH in different networks, observing that persistent topological attributes are related to the robustness of networks and reflect deficiencies in certain connectivity properties [S29]. Additionally, Jonsson’s book [S30] provides insights on how to construct a simplicial complex from a graph. Recently, Wu et al. applied a persistent variant of the GLMY homology for directed graphs of Grigor’yan, Lin, Muranov, and Yau to the study of networks of complex diseases [S31, S32].

#### S.4.2 Vectorising persistent homology for machine learning

When executing PH on point-cloud data, one typically obtains PD/PB, which is a set of intervals on the (extended real) line. Indeed, PD/PB can be considered a form of vectorisation of the original data. However, they may not be sufficiently accessible for further applications, such as integration into machine learning algorithms for future model development. Since the intervals exist on the extended line, some may involve  $+\infty$  as their terminal point, which can pose challenges for certain algorithms. This issue can be mitigated by setting a threshold for the maximal lifetime, which is a relatively straightforward solution. However, there are more intrinsic challenges embedded in the vectorisation of

<sup>2</sup>In order, they are available at

<https://mrzv.org/software/dionysus2>  
<https://bitbucket.org/phat-code/phat>  
<https://github.com/DIPHA/dipha>  
<https://giotto-ai.github.io/gtda-docs/0.4.0>

1498 PD/PB that are not easily resolved and may pose difficulties  
 1499 for researchers attempting to leverage this powerful tool.  
 1500 For example, the number of intervals in PD/PB is not fixed;  
 1501 sometimes, there may be 10, and other times there may be  
 1502 100. Moreover, PD is too sparse to put into machine learning  
 1503 algorithms. Researchers may extract the top five longest  
 1504 intervals from the set as a method of vectorisation, or  
 1505 remove intervals with a length less than a certain threshold  
 1506 from the set, or implement the distance functions and kernel  
 1507 methods of PD/PB to achieve vectorisation. In this article,  
 1508 vectorisation in TopCap is relatively simple, as we extract  
 1509 the MP and its corresponding birth time as two topological  
 1510 features to feed into machine learning algorithms.

1511 There is no definitive rule to determine that one method  
 1512 of vectorisation is superior to another, as the performance  
 1513 of vectorisation methods largely depends on the data and  
 1514 how they are transformed into a topological space. Indeed,  
 1515 there are a great many creative methods for vectorising PH.  
 1516 Persistence Landscapes (PL) [S33], developed by Bubenik,  
 1517 is one popular method. Bubenik's work introduces both  
 1518 theoretical and experimental aspects of PL in a statistical  
 1519 manner. Generally speaking, PL maps PD into a function  
 1520 space that is stable and invertible [S34]. A toolbox [S35] is  
 1521 also available for implementing PL. Persistence Image [S36],  
 1522 another vectorisation method developed by Adams et al.,  
 1523 stably maps PD to a finite-dimensional vector representation  
 1524 depending on resolution, weight function, and distribution  
 1525 of points in PD. For additional vectorisation methods, one  
 1526 may consider the article [S37] by Ali et al., which presents  
 1527 13 ways to vectorise PD.

## 1528 References for supplementary information

- 1530 [S1] Gunnar Carlsson et al. "On the local behavior of  
 1531 spaces of natural images". In: *International Journal*  
 1532 of *Computer Vision* 76 (Jan. 2008), pp. 1–12. DOI: 10.  
 1533 1007/s11263-007-0056-x.
- 1534 [S2] IPA Chart. *The international phonetic alphabet (revised to 2020)*. International Phonetic Association,  
 1535 retrieved 16th January 2024 from <https://www.internationalphoneticassociation.org/content/ipa-chart>.
- 1539 [S3] Jose A. Perea and John Harer. "Sliding windows and  
 1540 persistence: An application of topological methods  
 1541 to signal analysis". In: *Foundations of Computational*  
 1542 *Mathematics* 15.3 (June 2015), pp. 799–838. ISSN: 1615–  
 1543 3383. DOI: 10.1007/s10208-014-9206-z.
- 1544 [S4] Afra Zomorodian and Gunnar Carlsson. "Computing persistent homology". In: *Discrete & Computational Geometry* 33.2 (Feb. 2005), pp. 249–274. ISSN:  
 1545 1432-0444. DOI: 10.1007/s00454-004-1146-y.
- 1548 [S5] Edelsbrunner, Letscher, and Zomorodian. "Topological persistence and simplification". In: *Discrete &*  
 1549 *Computational Geometry* 28.4 (Nov. 2002), pp. 511–533.  
 1550 ISSN: 1432-0444. DOI: 10.1007/s00454-002-2885-2.
- 1552 [S6] Serguei Barannikov. "The framed Morse complex  
 1553 and its invariants". In: *Advances in Soviet Mathematics*.
- [S7] Vanessa Robins. "Towards computing homology from finite approximations". In: *Topology Proceedings*. Vol. 24. 1999, pp. 503–532.
- [S8] Afra Jozé Zomorodian. *Computing and comprehending topology: Persistence and hierarchical Morse complexes*. University of Illinois at Urbana-Champaign, 2001.
- [S9] Edelsbrunner, Letscher, and Zomorodian. "Topological persistence and simplification". In: *Discrete & Computational Geometry* 28.4 (2002), pp. 511–533. ISSN: 1432-0444. DOI: 10.1007/s00454-002-2885-2.
- [S10] Gunnar Carlsson et al. "Persistence barcodes for shapes". In: *International Journal of Shape Modeling* 11.02 (2005), pp. 149–187. DOI: 10.1142/s0218654305000761.
- [S11] Afra Zomorodian and Gunnar Carlsson. "Computing persistent homology". In: *Discrete & Computational Geometry* 33.2 (2005), pp. 249–274. ISSN: 1432-0444. DOI: 10.1007/s00454-004-1146-y.
- [S12] David Cohen-Steiner, Herbert Edelsbrunner, and John Harer. "Stability of persistence diagrams". In: *Proceedings of the twenty-first annual symposium on Computational geometry*. 2005, pp. 263–271.
- [S13] Gunnar Carlsson. "Topology and data". In: *Bulletin of The American Mathematical Society* 46 (Apr. 2009), pp. 255–308. DOI: 10.1090/S0273-0979-09-01249-X.
- [S14] Gunnar Carlsson and Mikael Vejdemo-Johansson. *Topological data analysis with applications*. Cambridge University Press, 2021. ISBN: 1108983944.
- [S15] Frédéric Chazal and Bertrand Michel. "An introduction to topological data analysis: Fundamental and practical aspects for data scientists". In: *Frontiers in Artificial Intelligence* 4 (2021), p. 108. ISSN: 2624-8212.
- [S16] Clément Maria et al. "The gudhi library: Simplicial complexes and persistent homology". In: *Mathematical Software—ICMS 2014: 4th International Congress, Seoul, South Korea, August 5–9, 2014. Proceedings*. Springer. 2014, pp. 167–174.
- [S17] Ulrich Bauer. "Ripser: Efficient computation of Vietoris-Rips persistence barcodes". In: *Journal of Applied and Computational Topology* 5.3 (2021), pp. 391–423. DOI: 10.1007/s41468-021-00071-5.
- [S18] Julien Tierny et al. "The topology toolkit". In: *IEEE Transactions on Visualization and Computer Graphics* 24.1 (2017), pp. 832–842. ISSN: 1077-2626.
- [S19] Brittany Terese Fasy et al. *Introduction to the R package TDA*. 2015. arXiv: 1411.1830 [cs.MS].
- [S20] Gurjeet Singh, Facundo Mémoli, and Gunnar E Carlsson. "Topological methods for the analysis of high dimensional data sets and 3D object recognition". In: *Eurographics Symposium on Point-Based Graphics* 2 (2007), pp. 91–100.
- [S21] Monica Nicolau, Arnold J Levine, and Gunnar Carlsson. "Topology based data analysis identifies a subgroup of breast cancers with a unique mutational profile and excellent survival". In: *Proceedings of the National Academy of Sciences* 108.17 (2011), pp. 7265–7270. ISSN: 0027-8424.
- [S22] Raúl Rabadán and Andrew J Blumberg. *Topological data analysis for genomics and evolution: Topology*

- 1615           *in biology*. Cambridge University Press, 2019. ISBN:  
 1616           1108753396.
- 1617 [S23] Saba Emrani, Thanos Gentimis, and Hamid Krim.  
 1618        “Persistent homology of delay embeddings and its  
 1619        application to wheeze detection”. In: *IEEE Signal  
 1620        Processing Letters* 21.4 (2014), pp. 459–463. ISSN: 1070-  
 1621        9908.
- 1622 [S24] Michael Robinson. *Topological signal processing*.  
 1623        Vol. 81. Springer, 2014.
- 1624 [S25] Woong Bae, Jaejun Yoo, and Jong Chul Ye. “Beyond  
 1625        deep residual learning for image restoration: Persistent  
 1626        homology-guided manifold simplification”. In: *Proceedings of the IEEE Conference on Computer Vision  
 1627        and Pattern Recognition Workshops*. 2017, pp. 145–153.
- 1628 [S26] Christoph Hofer et al. “Deep learning with topolog-  
 1629       ical signatures”. In: *Advances in Neural Information  
 1630       Processing Systems* 30 (2017).
- 1631 [S27] Ephy R. Love et al. “Topological convolutional layers  
 1632       for deep learning”. In: *Journal of Machine Learning  
 1633       Research* 24.59 (2023), pp. 1–35.
- 1634 [S28] Vin De Silva and Robert Ghrist. “Coverage in sensor  
 1635       networks via persistent homology”. In: *Algebraic &  
 1636       Geometric Topology* 7.1 (2007), pp. 339–358. ISSN: 1472-  
 1637       2739.
- 1638 [S29] Danijela Horak, Slobodan Maletić, and Milan Ra-  
 1639       jković. “Persistent homology of complex networks”.  
 1640       In: *Journal of Statistical Mechanics: Theory and Experi-  
 1641       ment* 2009.03 (2009), P03034. ISSN: 1742-5468.
- 1642 [S30] Jakob Jonsson. *Simplicial complexes of graphs*. Vol. 3.  
 1643       Springer, 2008.
- 1644 [S31] Shuang Wu et al. “The metabolomic physics of com-  
 1645       plex diseases”. In: *Proceedings of the National Academy  
 1646       of Sciences* 120.42 (2023), e2308496120. DOI: 10.1073/  
 1647       pnas.2308496120.
- 1648 [S32] Alexander Grigor’yan. “Advances in path homology  
 1649       theory of digraphs”. In: *Notices of the International  
 1650       Congress of Chinese Mathematicians* 10.2 (2022), pp. 61–  
 1651       124. ISSN: 2326-4810,2326-4845. DOI: 10.4310/ICCM.  
 1652       2022.v10.n2.a7.
- 1653 [S33] Peter Bubenik. “Statistical topological data analysis  
 1654       using persistence landscapes”. In: *Journal of Machine  
 1655       Learning Research* 16.1 (2015), pp. 77–102.
- 1656 [S34] Peter Bubenik. “The persistence landscape and some  
 1657       of its properties”. In: *Topological Data Analysis: The  
 1658       Abel Symposium 2018*. Springer, 2020, pp. 97–117.
- 1659 [S35] Peter Bubenik and Paweł Dłotko. “A persistence  
 1660       landscapes toolbox for topological statistics”. In: *Journal of Symbolic Computation* 78 (2017), pp. 91–114.  
 1661       ISSN: 0747-7171.
- 1662 [S36] Henry Adams et al. “Persistence images: A stable  
 1663       vector representation of persistent homology”. In: *Journal of Machine Learning Research* 18 (2017).
- 1664 [S37] D. Ali et al. “A survey of vectorization methods  
 1665       in topological data analysis”. In: *IEEE Transactions  
 1666       on Pattern Analysis and Machine Intelligence* (2023),  
 1667       pp. 1–14. ISSN: 1939-3539. DOI: 10.1109/TPAMI.2023.  
 1668       3308391.